PROCESSES UNDERLYING FRUIT CUTICLE INTEGRITY IN TOMATO (*SOLANUM* SPP.)

A Thesis

Presented to the Faculty of the Graduate School

of Cornell University

in Partial Fulfillment of the Requirements for the Degree of

Master of Science

by

Annelise Vieira

December 2023

ABSTRACT

The ability to synthesize, deposit and maintain a biomechanically resilient epidermis and a hydrophobic cuticle covering aerial organs are crucial protective features of all land plants. To achieve an intact and dynamic epidermal layer in growing tissues, the deposition of complex primary cell wall polysaccharides and structural cuticular lipids must involve complex and coordinated trafficking, assembly, and restructuring processes. In rapidly expanding organs, such as fleshy fruits, lack of coordination of these processes can result in cuticle and epidermal defects, manifested as cracking and corky scarring, which in crops can lead to substantial economic losses. Identification of the causes of such defects can also provide new insights into the molecular basis of systems to maintain epidermal integrity. As an example, the tomato *HYPERCRACKING 1 (hcr1)* mutant shows extensive fruit cracking at an early developmental stage, and consequent massive deposition of suberin in the epidermis during growth. Map-based cloning of the *hcr1* locus and biochemical analysis suggested that the hyper-cracking phenotype is a consequence of defective sterol biosynthesis. Morphological, cytological, and molecular characterization of *hcr1* fruit revealed inhibited cell expansion and division in the pericarp and reduced cellulose levels leading to impaired pericarp development, resulting in uncoordinated expansion between the pericarp and the inner tissues leading to cracking. This study suggests that sterols are important for primary cell wall deposition, and notably cellulose synthesis. Moreover, the presence of a strong cracking phenotype in fruit, but not vegetative tissues, highlights variability in the susceptibility of different organs to impaired epidermal integrity.

Relatedly, a second study is concerned with microscopic pores associated with trichomes on the fruit cuticle that are exposed when trichomes are dislodged. Staining of the pore areas with Toluidine Blue has shown that they have the capacity to become sealed, an adaptation with

implications for water retention and relevant to open research questions regarding cuticle structure and remodeling. The South American tomato relative *Solanum quitoense* (common name: naranijlla) displays large, abundant, and uniformly spaced trichomes on the fruit surface, and here we used this expedient model for studying the sealing process. Evapotranspiration experiments revealed that removal of trichomes at harvest significantly increases fruit water loss, confirming that the trichome pores are significant routes of water loss, as in *S. lycopersicum.* However, isolated cuticles that have been allowed to seal prior to isolation allow less transcuticular water loss than those isolated immediately after trichome removal, indicating that pore sealing effectively inhibits this water loss through pores. Staining the cuticle with Toluidine Blue and imaging the surface revealed that the area of the pore stain gets measurably smaller with sealing time, plateauing at approximately 3 days. Viewing these stained pores at cross section, contextualized to SEM images, suggests that the sealing does not occur at the surface of the trichome scar, but rather along the base of the exposed cavity. Evidence of the sealing mechanism was not captured by confocal microscopy and staining with Basic Fuchsin, Fluorol Yellow, and Calcofluor White, possibly due to the complexity of the *S. quitoense* cuticle architecture and the lack of specificity of stains primarily characterized in *Arabidopsis*. This rules out, however, that the sealing mechanism involves a large (>10 micrometer) material deposit, as this would have been detectable. Additional study will be necessary to understand the mechanism of this sealing process and to determine whether these findings generalize to tomatoes of greater commercial interest, especially *S. lycopersicum*.

BIOGRAPHICAL SKETCH

Annelise Vieira graduated from Palm Harbor University High School with an International Baccalaureate Diploma. She then completed a Bachelor of Science degree in Plant Science at the University of Florida, with a specialization in Plant Breeding and Genetics and a minor in Bioinformatics. Annelise was awarded the National Science Foundation Graduate Research Fellowship in 2021 and is also serving as a 2023 Plantae Fellow of the American Society of Plant Biologists.

ACKNOWLEDGEMENTS

I am deeply thankful for many who have made this work possible, especially my advisor, Dr. Jocelyn Rose, whose thorough discussion, patient support, and concern were crucial for my completing this work and growing from the experience. I am also especially grateful for Dr. Iben Sørensen for her generous and patient help and mentorship in the lab. Further, many of my coworkers in the Rose lab, including Dr. Aurore Guerault, Milay Haskin, and Stephen Snyder offered thoughtful help, collaboration, and discussion. A former member of the lab, Dr. Yonghua He, is due much credit for collecting the bulk of the data comprising Chapter 1 of this work, along with his collaborators Dr. Sonia Osorio-Algar, Dr. Tal Isaacson, and Dr. Alisdair R. Fernie. He was also assisted by Dr. D. Zamir's providing *hcr1* tomato seeds, and by Nancy Eannetta, Yimin Xu and Dr. Bin Cong with map-based cloning in Dr. Tanksley's lab. I am also grateful for my committee members, Dr. Jim Giovannoni and Dr. Margaret Frank for their flexibility and support, as well as the labs of Dr. Alejandra Gandolfo Nixon and Dr. David Domozych for hospitality and sharing of their microscopes and expertise. Friends, family, and community have also sustained and affected me profoundly during this time.

TABLE OF CONTENTS

INTRODUCTION

Losses of fresh produce in the United States to postharvest spoilage reach up to 50% of economic value, much of which is attributable to desiccation, pests, and pathogens (Buzby et al., 2011). The primary barrier against these threats is a plant's cuticle, the extracellular hydrophobic layer that covers the aerial epidermis of all land plants (Martin and Rose, 2014). The cuticle serves several functions crucial to plant survival on land, including regulating water loss and uptake, protecting against UV radiation, providing mechanical support, preventing pathogen infection, and maintaining organ boundaries. This water retention and protection against pathogens is important in determining shelf life postharvest, and its contribution to crops' appearance and palatability affects their commercial viability (Yeats and Rose, 2013). Thus, the plant cuticle plays a vital role in issues of sustainability and food security.

The basic structure of the plant cuticle consists of a structurally complex lipidic polyester, termed cutin, as well as polysaccharides and various soluble compounds that are referred to collectively as waxes (Schreiber, 2010; Yeats and Rose, 2013). Cuticle composition varies widely across plant species and organs, with corresponding variability in traits such as permeance. An excellent model to study the biochemical, biophysical and regulatory systems that contribute to plant organ surface integrity is the expansion of tomato (*Solanum lycopersicum* L.) fleshy fruit, which have a thick, astomatous cuticle, and exhibit rapid expansion during development (Petit et al., 2021). Further, tomato is among the most produced fruit and vegetable crops in the United States and is also highly prone to postharvest transpirational water loss and spoilage, making it a major contributor to food waste (Buzby et al., 2011).

A major research aim is to understand precisely how specific cuticle components, the cuticle's architecture, and mechanisms of cuticle assembly and remodeling contribute to forming an integrated cuticle capable of performing its protective functions. While many enzymes and pathways involved in the biosynthesis of cuticle precursors have been characterized, the mechanisms by which these compounds are then trafficked, deposited, assembled, built into distinct architectural patterns, and restructured remain largely unknown (Martin and Rose, 2014; Fich et al., 2016; Philippe et al., 2021). For instance, how is the integrity of the surface maintained as the fruit expands? The coordination between cuticle deposition and the formation and restructuring of the load-bearing polysaccharide primary cell wall is not understood, but it must involve complex processes that accommodate the demands of growth and development. Relatedly, in what ways may the cuticle be able to respond to damages throughout and after development? How the cuticle may integrate new material or remodel its existing architecture in response to damage is relevant to developing crops resilient to environmental stressors.

Toward answering these questions, this thesis presents two works dealing with compromised surface integrity in tomato fruit. The first identifies the genetic basis of a tomato mutant that shows extensive fruit cracking at an early developmental stage. Much of the initial data for this work was generated by former Rose lab student Dr. Yonghua He, which I confirmed via a CRISPR knockout, reproduced cell wall analyses, and tissue staining. The second work is concerned with trichome-associated pores in the tomato cuticle and seeks to characterize the process by which they become sealed using a wild relative as an experimental model system.

CHAPTER 1:

Characterization of the Tomato *HYPERCRACKING 1 (hcr1)* Mutant Underscores the Importance of Sterols in Cellulose Biosynthesis and Fruit Surface Integrity

INTRODUCTION

Approximately 450 million years ago, freshwater plants developed the capacity to colonize terrestrial habits, which necessitated adaptation to more extreme temperatures, desiccation, biomechanical stresses and heightened UV radiation exposure (Waters, 2003; Leliaert et al., 2011; McCourt et al., 2023). This involved the evolution of various morphological and physiological traits, which can be seen in both the fossil record and extant plant lineages; for instance, architecturally complex cell walls, essential for support, originated in the Charophycean green algae (Sørensen et al., 2011), the sister lineage of land plants. Crucially, the ability to retain water in drying habitats led to the development of a hydrophobic surface layer, or cuticle. Composed principally of the polymer cutin and cuticular waxes, the cuticle performs diverse and vital functions in plant development and environmental stress resistance, including minimizing water loss, providing mechanical support, protecting against UV radiation and pathogens, and maintaining organ integrity (Yeats and Rose, 2013). Today, all land plants synthesize, deposit, and maintain a cuticle over all aerial organs as well as the root cap, allowing them to thrive in otherwise desiccating environments (Berhin et al., 2019).

While many enzymes and pathways involved in the biosynthesis of cuticle precursors have been characterized, the mechanisms by which these compounds are then trafficked, deposited, assembled, built into distinct architectural patterns, and restructured remain largely unknown

(Martin and Rose, 2014; Fich et al., 2016; Philippe et al., 2022). Notably, the coordination between cuticle deposition and the formation and restructuring of the load-bearing polysaccharide primary cell is unresolved, but it must involve complex processes that occur throughout growth and development, in response to the biomechanical demands and tensile stresses in the epidermis. Failure to coordinate these processes inevitably leads to a loss of surface integrity and so studying examples of epidermal disruption can provide insights into the underlying molecular mechanisms.

An excellent model to study the biochemical, biophysical and regulatory systems that contribute to plant organ surface integrity is the expansion of tomato (*Solanum lycopersicum* L.) fleshy fruit, which have a thick, astomatous cuticle, and exhibit rapid expansion during development, as well as readily identified phenotypes when the epidermis is disrupted (Petit et al., 2021). Fruit cracking and 'catfacing' (corky scars on the fruit surface) cause significant economic loss by reducing fruit quality and insect and pathogen resistance (Peet, 2009), as reported studies of tomato, cherry (*Prunus avium*), pomegranate (*Punica granatum*), apple (*Malus domestica*), watermelon (*Citrullus lanatus*), grape (*Vitis vinifera*), and litchi (*Litchi chinensis*) (Santos et al., 2023). It has been suggested that cracking occurs when fruit tissues are subjected to pressures that exceed the mechanical resistance provided by their cuticle and cell walls (Brüggenwirth and Knoche, 2017). Environmental factors can increase the incidence of cracking: for instance, high rainfall and high temperatures make fruit more prone to cracking by reducing the tensile strength of the fruit cuticle and causing rapid growth (Kamimura et al., 1972; Butani et al., 2019). Anatomical characteristics conferring cracking susceptibility in tomato include large fruit size, low cuticle tensile strength and/or low cuticle extensibility at the turning to pink stage of

ripeness, thin ‘skin’, thin pericarp, shallow cutin penetration, few fruit per plant, and fruit that are unshaded by foliage (Peet, 1992). In recent studies seeking to understand the causes of cracking, expression analyses have indicated that many gene families that may be involved, including those involved in cutin biosynthesis and deposition, cuticular wax biosynthesis, cuticular membrane and cell wall biosynthesis, suberin and lignin biosynthesis, hormone metabolism, water transport, calcium transport and signaling, and starch and sucrose metabolism, as well as different transcription factors (Santos et al., 2023). Notably, genes involved in cell wall metabolism significantly affect fruit cracking susceptibility (Wang et al., 2021), and it has been shown that the cracking rate is influenced by the protopectin and cellulose content of cell walls in tomato, as well as the pericarp structure in cherry (Brüggenwirth and Knoche, 2017; Jiang et al., 2019). Although the precise genetic bases and physiology of cracking remain mysterious, it is clear that the coordination of polysaccharide cell wall and cuticle structure is crucial in maintaining an intact fruit surface during expansion.

To shed light on processes that maintain organ integrity during expansion and to investigate the underlying molecular bases, a search was performed online of the ‘Genes that Make Tomatoes’ collection (Menda et al., 2004) for mutants annotated as exhibiting a fruit cracking phenotype. One mutant (#e4702m1), exhibiting extensive fruit cuticle cracking, was identified and named *hypercracking1* (*hcr1*). Genetic analyses revealed that the causal gene was involved in sterol biosynthesis, uncovering an underappreciated link between sterol biosynthesis and fruit surface integrity.

RESULTS

The *hcr1* mutant shows phenotypes and metabolic abnormalities associated with early fruit cracking and suberization

The *hcr1* mutant's distinct cracking phenotype was identified in a screen of the 'Genes that Make Tomatoes' EMS mutagenesis collection (Menda et al., 2004). *Greenhouse grown hcr1* plants were phenotypically normal during vegetative growth although subtle phenotypes were observed, such as necrotic spots gradually developing on some of the newly emerging leaves after the emergence of the first inflorescence and some necrosis on the surface of some of the anthers (Figure S1a,c). The major phenotypes, however, occurred on the *hcr1* fruit, and consisted of surface discoloration, cracking, suberization, and reduced expansion (Figure 1a-d). Fruit *discoloration* occurred as early as 3 days after pollination (DAP) and all fruit exhibited some discoloration by 6 days after pollination (DAP) (Figure 1b, S1b). The first visible cracks were generally seen 3-5 days after the appearance of discoloration (Figure 1b, S1d). However, the most striking *hcr1*phenotype was the deposition of large, suberized scars on the fruit (Figure 1a), which typically occurred coincident with the cracks, indicating that the suberization was a wound response.

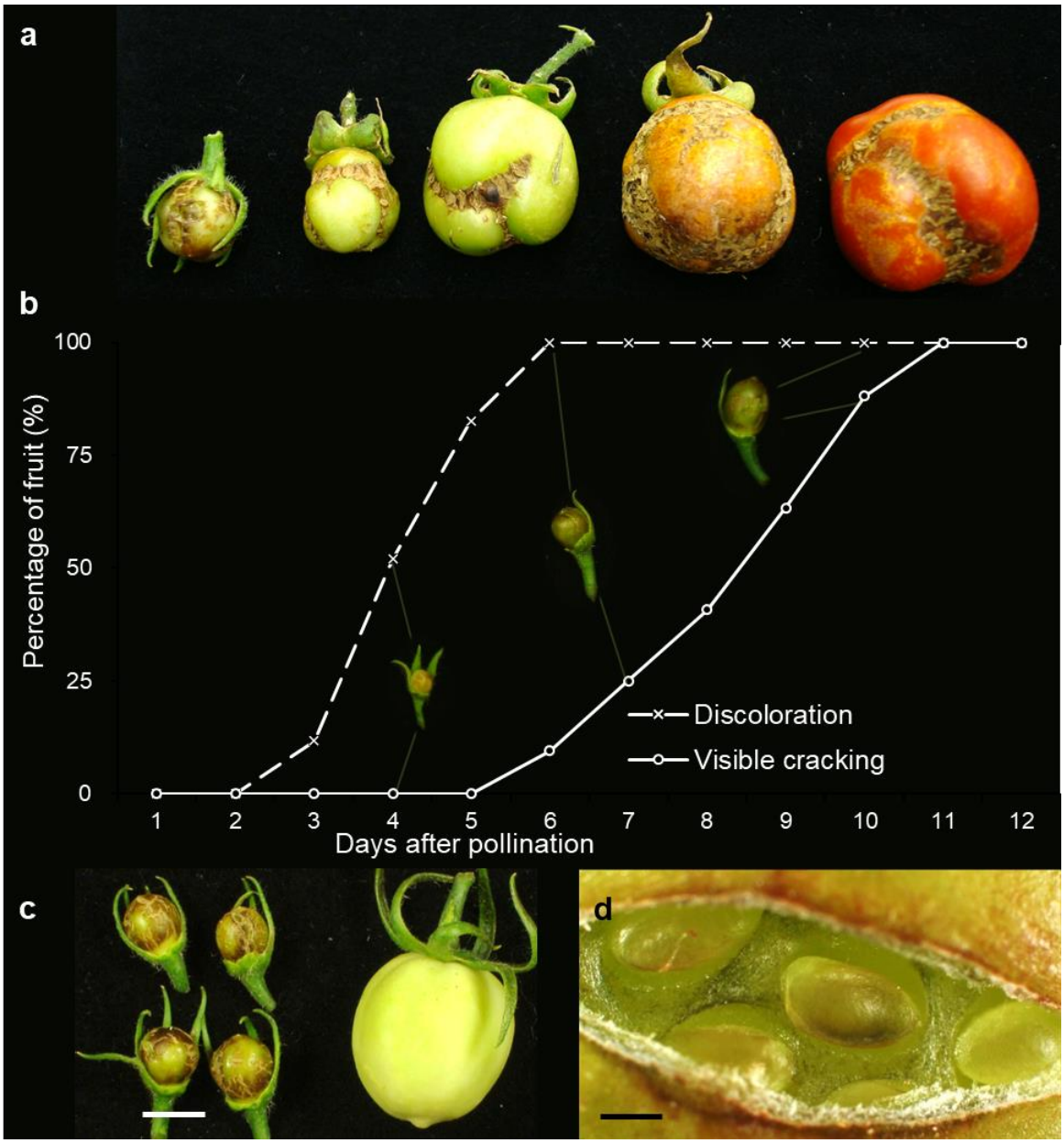

Figure 1. The fruit phenotypes of the *hcr1* mutant. (a) *hcr1* fruit at various stages of development and ripening displaying large cracks and suberization. Stages in (b) from top to bottom: 10 DAP, 20 DAP, mature green, pink pericarp, red ripe. (b) Time course of the occurrence of discoloration or visible cracks on the *hcr1* fruit surface with photos of *hcr1* at 4, 7, and 10 DAP. (c) Comparison of fruit sizes between *hcr1* (left) and M82 (right) at 14 DAP. (d) Large crack on *hcr1* fruit. Scale bars: (a, c) = 1 cm, (d) = 500 µm. Data collected by Dr. Yongua He (YH).

The wide range of phenotypic traits shown by *hcr1*, including fruit discoloration, suberin deposition, abnormal cuticle development, and inhibited cell division and expansion suggested that many metabolic pathways were altered by the *hcr1* mutation (Figure 2a-f). To confirm this, the expression patterns of several marker genes related to these processes were investigated.

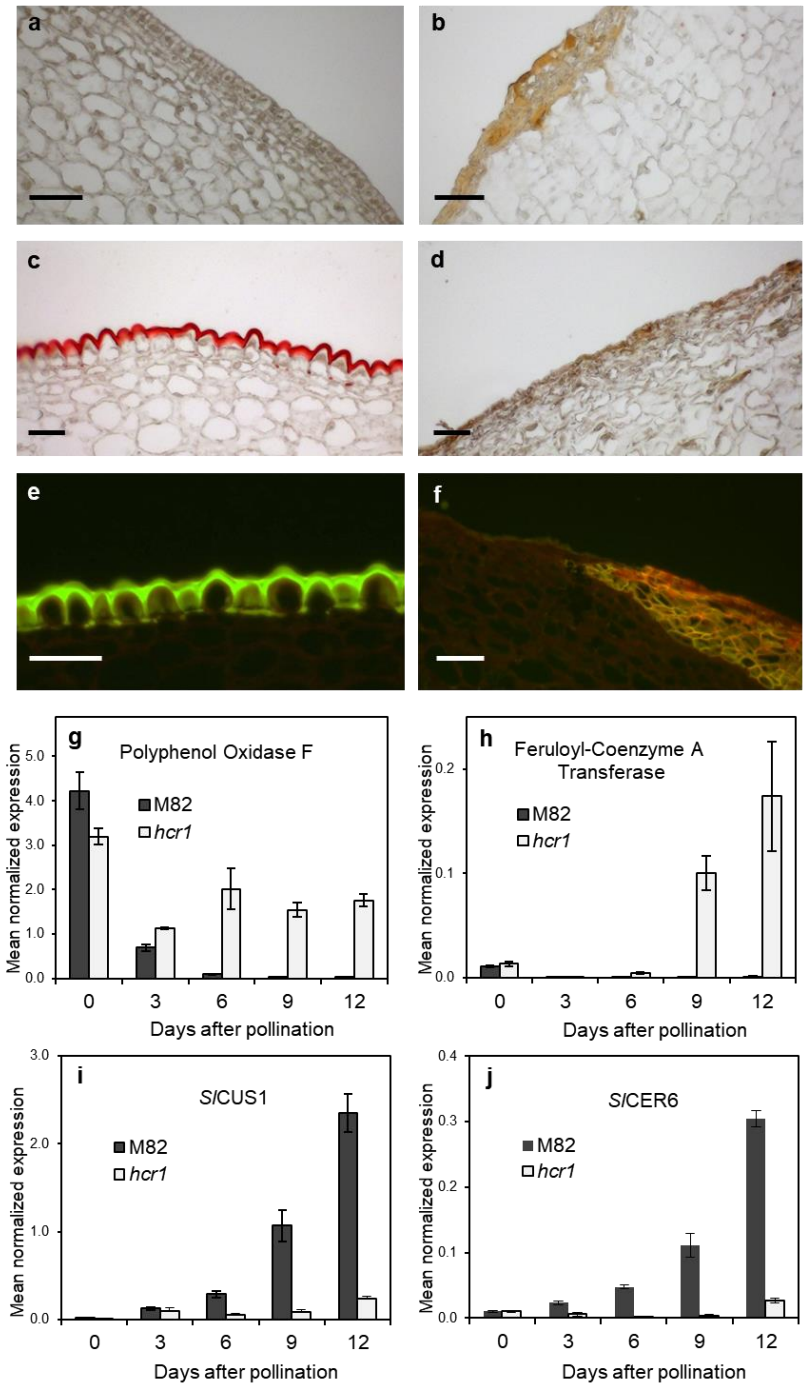

Figure 2. Light microscopy images of *hcr1* fruit pericarp tissues. (a-b) Fruit pericarp cross sections of M82 (a) and *hcr1* (b) at 7 DAP, stained with Sudan IV, showing disordered epidermal cells with thickened cell walls in *hcr1*. (c-d) Fruit pericarp cross sections of M82 (c) and *hcr1* (d) at 14 DAP, stained with Sudan IV, showing the developing cutin layer in M82 (c), but almost no cutin layer in *hcr1* (d). (e-f) Fluorescence images of fruit pericarp cross sections at 21 DAP, stained with neutral red, showing a well-developed cutin layer in M82 (e) and the suberized tissues in *hcr1* (f). Scale bars (a-f) = 50 µm. (g-h) The expression patterns of marker genes related to fruit discoloration, suberization and cuticle biosynthesis

in fruit pericarp by qPCR. (g) The expression of Polyphenol Oxidase F, which was used as a measure of phenolic compound formation. (h) The expression of Feruloyl-Coenzyme A Transferase, which was used as a measure of suberin biosynthesis. (i) The expression of the cutin polymerase *Sl*CUS1 gene as a measure of cutin biosynthesis. (j) The expression of the *Sl*CER6 gene as a measure of cuticular wax biosynthesis. Data collected by YH.

Mechanical wounding and pathogen infection can induce the expression of the *PPO-F* gene, which is a polyphenol oxidase catalyzing the O2-dependent oxidation of phenolics to quinones, the secondary reaction of which can lead to the formation of polymeric brown or black pigments (Thipyapong et al., 1997, 2007). This gene may therefore be involved in the observed brown discoloration of the *hcr1* fruit, and quantitative (q) PCR analysis of PPO-F expression (Figure 2g) indicated that while unpollinated fruit had the highest levels of PPO-F transcripts, after pollination transcript abundance decreased dramatically to 1-4% of the original 0 DAP levels in wild type (M82) fruit. In contrast, PPO-F transcript levels in *hcr1* fruit remained almost as high as at 0 DAP during this period and were about 60-fold greater than that of M82 wild type, which is consistent with PPO-F contributing to the fruit discoloration in *hcr1*.

Given the highly suberized appearance of the *hcr1* fruit, we also investigated the expression of the key suberin biosynthesis enzyme feruloyl-CoA transferase (Solyc03g097500.2), a homolog of which has been shown in *Arabidopsis thaliana* (AT5G41040) to be essential for the incorporation of ferulate into suberin (Molina et al., 2009). qPCR results showed that this gene was consistently expressed at a very low level in M82 fruit but was substantially upregulated in *hcr1* from 6 DAP onwards in comparison with the wild type (Figure 2h), consistent with the observation that suberin synthesis follows the appearance of fruit cracks and discoloration.

Two marker genes associated with cutin and wax biosynthesis were also selected to evaluate cuticle formation in *hcr1* fruit. *Sl*CUS1 catalyzes the polymerization of cutin *in situ* via successive trans-esterification of 2-MHG to the growing cutin polymers (Yeats et al., 2012), while *Sl*CER6 encodes an essential enzyme of the very-long-chain fatty acid (VLCFA) elongase complex required for aliphatic wax biosynthesis (Vogg et al., 2004; Leide et al., 2007) and so its expression would be expected to correlate with wax deposition. The qPCR results revealed quite similar expression patterns of *Sl*CUS1 and *Sl*CER6 in M82 with both genes maximally expressed during the rapid expansion phase of fruit at 12 DAP or later (Figure 2i, 2j). In contrast, the expression of these two genes in *hcr1* fruit were substantially lower than in M82, suggesting that, as observed microscopically, cuticle development was delayed in the *hcr1* mutant.

Abnormal tissue and organ development of *hcr1* fruit is associated with inhibited cell expansion and division

Looking at the epidermal layers with light microscopy revealed misshapen cells with aberrant cell wall thickenings near the epidermis in *hcr1* fruit, in contrast to well-organized epidermal cells of M82 (Figure 2a,b), and the *hcr1* cuticle layer was significantly thinner than that of M82, suggesting a defect in cuticle development (Figure 2c,d). Substantial suberization was apparent associated with the cracked areas of *hcr1* fruit in contrast to the intact and unsuberized cuticle in M82 (Figure 2e,f). It was also apparent that the *hcr1* pericarp was far thinner and had much smaller (or sometimes absent) locular cavities than the wild type (Figure 3a), and the average size of *hcr1* pericarp parenchyma cells in cross section was substantially less than that of the wild type (Figure 3b,c), indicating an inhibition of cell expansion in *hcr1* fruit.

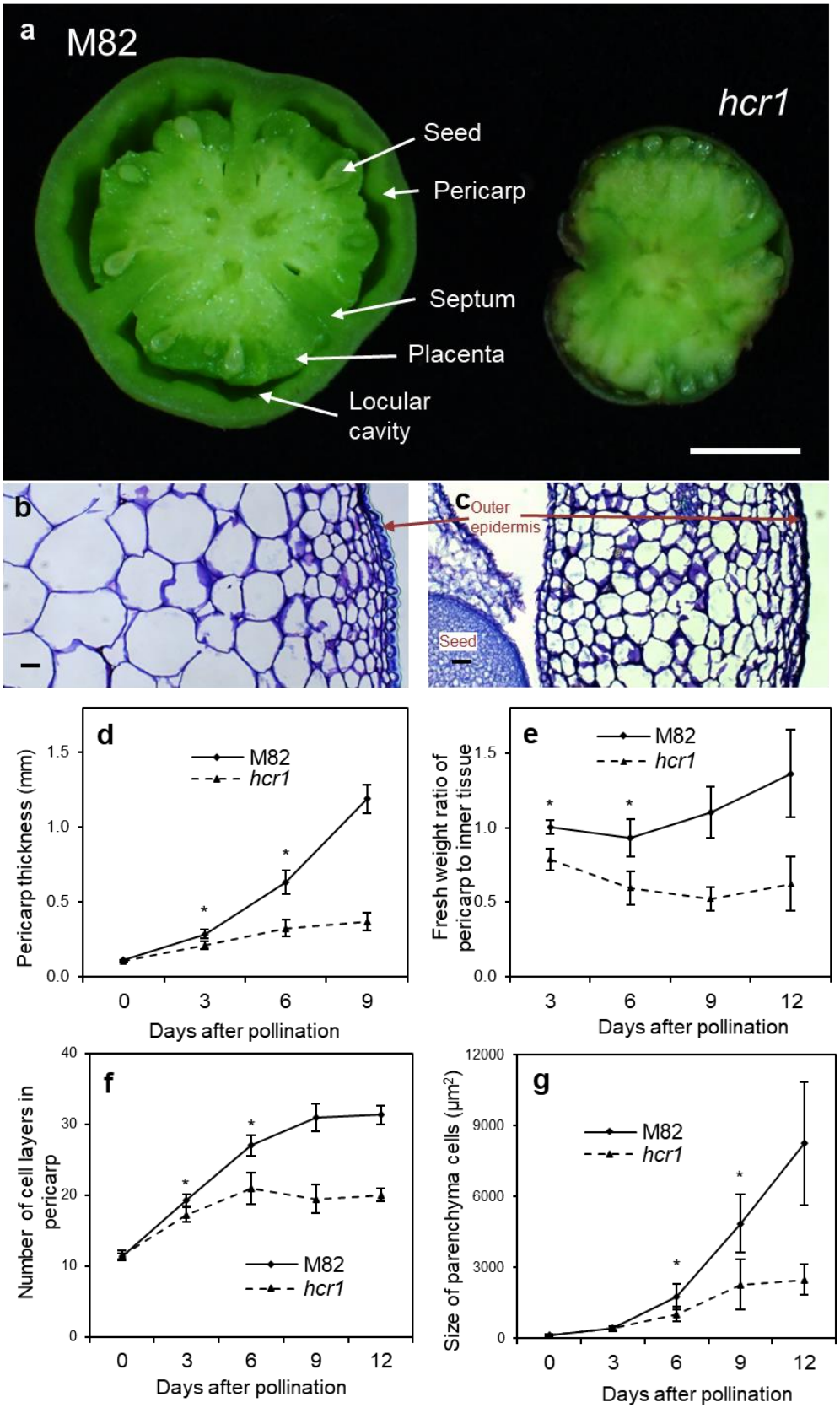
a
M82
hcr1
Seed
Pericarp
Septum
Placenta
Locular cavity
b
c
Outer epidermis
Seed
d
M82
hcr1
Pericarp thickness (mm)
Days after pollination
e
Fresh weight ratio of pericarp to inner tissue
Days after pollination
f
Number of cell layers in pericarp
Days after pollination
g
Size of parenchyma cells (μm²)
Days after pollination

Figure 3. Inhibited fruit pericarp development in *hcr1.* (a) Fruit cross sections of *hcr1* and M82 at 14 DAP. Scale bar = 1 cm. (b, c) Light microscopy images of pericarp cross section from M82 (b) and *hcr1* (c) fruit at 14 DAP in the same magnification, showing inhibition of cell expansion in *hcr1*. Scale bars = 100 μm. (d) Pericarp thickness in *hcr1* and M82. (e) Fresh weight ratio of pericarp to inner tissue of fruit in *hcr1* and M82. (f) Number of cell layers of *hcr1* and M82 pericarp. (g) Average areas of pericarp parenchyma cells in *hcr1* and M82 fruit. (Mean ± SD of N ≥ 8; * P < 0.01 by two-tailed t-test). Data collected by YH.

The anatomical abnormalities were quantified by measuring the pericarp thickness (Figure 3d), which showed no difference between *hcr1* and wild type at 0 DAP (ovary wall) but significant differences ($P<0.01$) by 3 DAP finally resulting in a 80% reduction by 9 DAP (Figure 3d). Also the ratio of pericarp fresh weight versus the weight of the inner tissues differed and was substantially smaller in *hcr1* than in M82 at 3 DAP (Figure 3e). The ratio continued to decline until 9 DAP in *hcr1* fruit in contrast to M82 where it continued to increase throughout the time course. These results confirmed that *hcr1* fruit pericarp growth was significantly inhibited compared with wild type fruit, and to determine whether this was a consequence of defective cell expansion or division, the number of pericarp cell layers was counted, and the parenchyma cell sizes were measured (Figure 3f, 3g). No differences were seen in the number of cell layers in the ovary wall at 0 DAP, but a significant ($p<0.01$) reduction was observed in *hcr1* by 3 DAP compared to M82. There was a substantial difference (approximately a 30% reduction) from 6 DAP onwards (Figure 3f), indicating that the *hcr1* mutation caused a disruption in cell division. The average area of pericarp parenchyma cells (Figure 3g), showed no difference between mutant and wild type at 0 and 3 DAP, but by 12 DAP the average area of an *hcr1* parenchyma cell was less than 30% that of M82, indicating a severe inhibition of cell expansion.

Genetic mapping identifies a mutation in the *HCR1* locus

The *hcr1* locus was first mapped to the middle portion of tomato chromosome two with a substantial QTL (LOD=32) between the CAPS markers 1g11430 (2.070) and 2g18030 (2.083) (Figure S2a, S2b). Following a screen of approximately 6,000 F_2 individuals for recombination events by the two markers, the gene locus was further narrowed down to a 42 kb interval between two flanking CAPS markers: Seq19600 and UDP4F within a BAC contig (corresponding to C02.40_contig20 in version 2.4 of tomato BAC contigs database, http://solgenomics.net) (Figure S2c). Genetic mapping led to the identification of a point mutation at the *HCR1* locus (See materials and methods, Figure 4a). This nucleotide substitution (G→A) was located to the predicted 3' splicing site of the seventh exon of the *HCR1* gene, resulting in the removal of the seventh exon from the mRNA, as subsequently confirmed by RT-PCR (Figure 4b). The chromosomal position of *HCR1* is SL2.40ch02:40139750…40146827.

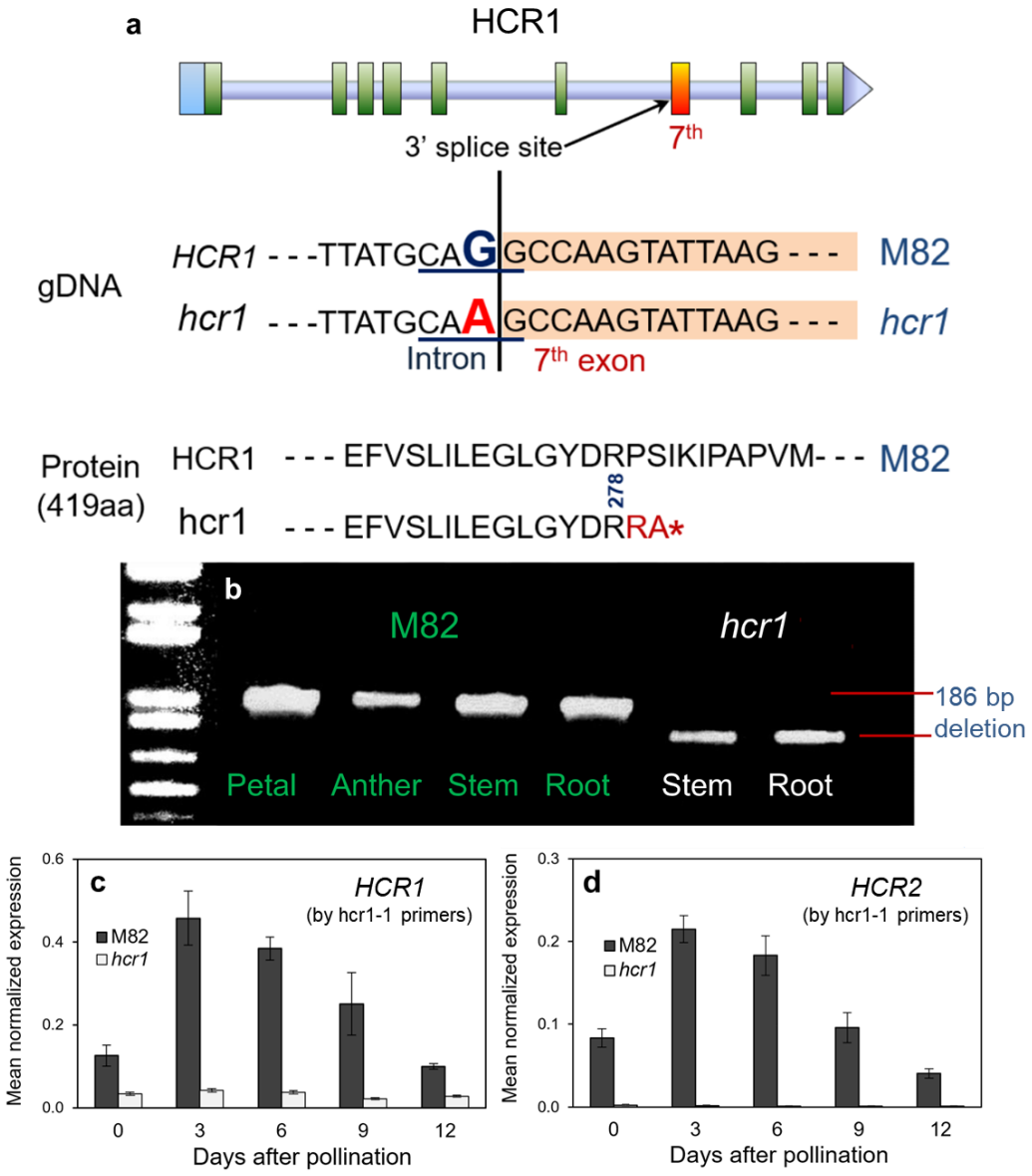

Figure 4. HCR1 gene model and PCR expression data. (a) *HCR1* gene model. The nucleotide substitution G to A at the 3' splice site results in the removal of the seventh exon from the mRNA of the gene, leading to the truncation of the last 142 amino acids from the protein. (b) RT-PCR of the HCR1 gene in M82 and *hcr1*, showing the 186 bp deletion in the mutant. (c,d) Developmental expression analyses of *HCR1* and *HCR2* transcripts in fruit pericarp by qPCR: *HCR1* gene expression was determined using (c) the hcr1-1 primer set, which is near to the 3'UTR region of the cDNA to detect all cDNA species, and (d) the hcr1-2 primer set, which is designed to detect the presence of the deleted seventh exon in cDNA of the *hcr1* mutant. Data collected by YH.

To validate the identity of the *HCR1* gene, complementation was performed using two plasmids: (i) CaMV35S::*HCR1* cDNA and (ii) Native Promoter::*HCR1* cDNA. All defective phenotypes of *hcr1*, including fruit discoloration, early cracking and cuticle suberization were entirely absent in the transgenic plants (T_0) transformed with either of the complementation constructs (Figure S3a-c). Segregation analysis in the subsequent generation (T_1) revealed that the progenies of selected transgenic (T_0) lines showed approximately 3:1 segregation ratios. In addition, a Clustered Regularly Interspaced Short Palindromic Repeats (CRISPR) *HCR1* knockout line phenocopied *hcr1* mutant phenotype in both the T_0 and T_1 generations (Figure S3c). Thus, it was confirmed that the single nucleotide mutation in the splicing site of the seventh exon of the *HCR1* gene was responsible for the *hcr1* phenotypes.

Two sets of *HCR1*-specific primers were designed matching two specific regions on the ninth and tenth exon (spanning the ninth intron). These were used to detect all *HCR1* cDNA species and the *hcr1*-2 primers, matching two specific regions on seventh and eighth exon (spanning the seventh intron), were used to detect the presence or absence of the deleted seventh exon of the *hcr1* gene. qPCR showed that the *hcr1* transcripts in the mutant were reduced to only about 10% of that of M82 at 3-9 DAP (Figure 4c); however, low levels of wild type *HCR1* transcripts with the seventh exon region intact were detected, albeit only at 0.5-1% of wild type levels (Figure 4d). A possible explanation for this result is that most *hcr1* mRNAs (about 90%) without the 7^{th} exon were eliminated by cellular quality control machineries due to the instability of the defective mRNA, but that very small amounts (0.5-1%) of functional *HCR1* mRNA accumulated in the *hcr1* mutant because of fault-tolerant splicing during mRNA transcription. It is noteworthy that the gene expression pattern in M82 fruit determined by the two sets of PCR primers showed

a similar pattern: *HCR1* gene expression levels peaked at 3 DAP then declined gradually during fruit development and were reduced to about 20% of peak values at 12 DAP.

The *HCR1* gene is highly expressed in tissues undergoing rapid cell expansion and division

The spatial and developmental expression pattern of the *HCR1* gene was next assessed using the β-glucosidase (GUS) reporter driven by the *HCR1* gene promoter. The results indicated that the *HCR1* gene is ubiquitously expressed in all tomato tissues (Figure S4). In fruit, GUS accumulation was relatively low in fruit pericarps at 1 DAP (Figure 5a), but quickly peaked by 3-5 DAP (Figure 5b). Expression was less in older fruit: there was no expression in some parenchyma cells at 12 DAP (Figure 5c), and expression was sporadic in mature green (Figure 5d) and red ripe (Figure 5e) fruit, only appearing in some cells near the epidermis and in vascular tissues. In stems, GUS staining was detected in all cells and was particularly abundant in young stem tissues (Figure S4a-d), then gradually declined as the tissues aged until staining was no longer detectable in older stem tissues. *HCR1* gene expression in petioles showed a similar developmental pattern to that in stems (Figure S4e-h). It was concluded from these expression analyses that the *HCR1* gene is abundantly expressed in the regions undergoing rapid cell division and expansion, and that the high expression early in fruit development is consistent with the appearance of early fruit cracking in the *hcr1* mutant.

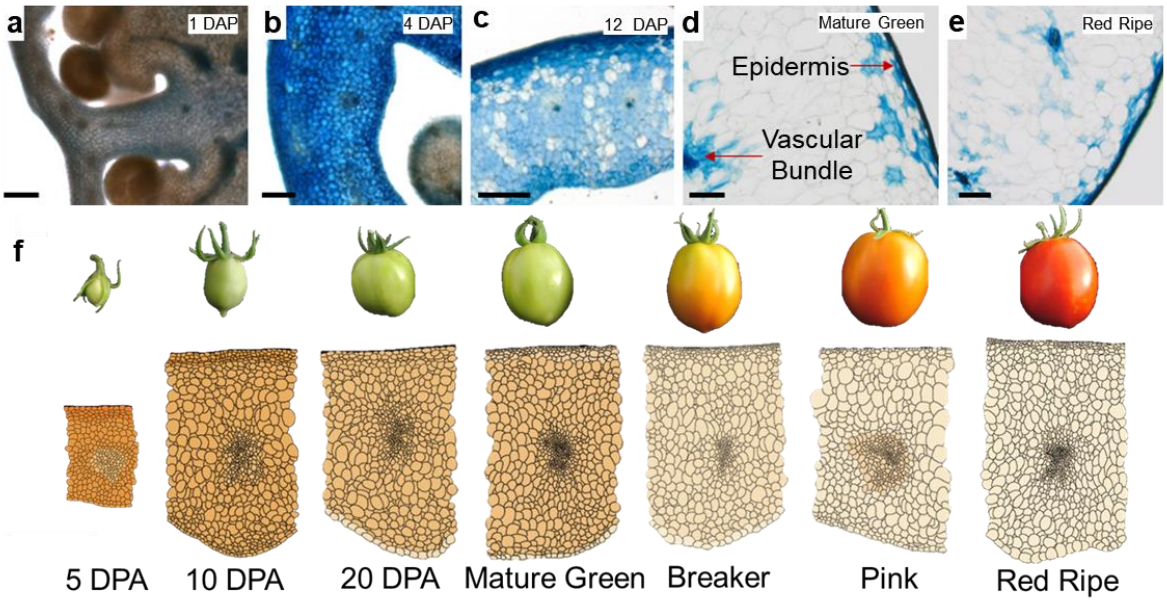

Figure 5. HCR1 gene family and expression patterns. (f) Representations of tomato pericarps through development with shading representing HCR1 expression level in the pericarp tissue via RNA-seq, which peaks with a value of 147.32 at 5 DPA and declines to 4.2 by the Red Ripe stage. Scale bar = 1 mm. Spatial and developmental expression analysis of *HCR1* gene using the GUS reporter system. (a-e) GUS staining of fruit pericarp at different stages: 1 DAP (a), 4 DAP (b), 12 DAP (c), mature green (d) and red ripe (e). Scale bars (a, b) = 100 µm, (c-e) = 500 µm. GUS data collected by YH.

To gain further insights into the exact *HCR1* expression patterns in different fruit tissues, the RNA-Seq data available in the SGN-Tomato Expression Atlas (SGN-TEA) (https://tea.solgenomics.net/) were used (Figure 5f). HCR1 was expressed at low levels in all tissues in the SGN-TEA dataset, including the seeds, columella, placenta, locular tissue, septum, inner epidermis, vascular tissue, parenchyma, collenchyma, and outer epidermis. In the fruit pericarp *HCR1* expression peaked at 5 DPA and declined throughout fruit expansion and ripening (Figure 5a). This pattern was consistent with the trends observed in qPCR analysis (Figure 4c,d).

The *HCR1* gene (Solyc02g081730) is predicted to encode a 419 amino acid polypeptide that bears a conserved 3β-HSD multi-domain pfam01073 (8-283aa, $7.61e^{-93}$). A BLAST search

against the *Arabidopsis* protein database showed that the tomato HCR1 protein exhibits a 78% sequence identity with *Arabidopsis* 3β-Hydroxysteroid Dehydrogenases/C-4 Decarboxylases (At3β-HSD1). HCR1 contains conserved glycine and aspartic residues, $TGGXGXXAX_{18}D$ near the N terminus, which are required to form the coenzyme-binding site (Rahier et al., 2006), and the highly conserved YX_3K segment [156-160aa], assigned to the catalytic center, is also present in *HCR1* (Jornvall et al., 1995; Rahier, 2011). A transmembrane helix [379-413aa] close to the C-terminal was predicted by TMHMM 2.0 (https://services.healthtech.dtu.dk/services/TMHMM-2.0/) and a putative ER retention and retrieving signal, the KSKKN motif of type-I ER membrane proteins, was found at the C-terminus (http://elm.eu.org/). In the *hcr1* mutant, removal of the seventh exon from the *HCR1* mRNA leads to the truncation of the last 142 amino acids (from 278aa to 419aa) from the protein (Figure 4a), which would almost certainly result in the loss of activity and correct subcellular localization.

The protein encoded by *HCR1* was identified as 3βHSD2 by Sonawane et al. (2016), who predicted that both it, and its homolog 3βHSD1 (Solyc04g082750), share the functions of two previously characterized *Arabidopsis* 3β-HSD isoenzymes (Rahier et al., 2006; 2009; Rahier, 2011; Sonawane et al., 2016). The At3β-HSDs are bifunctional short-chain proteins with 3β-hydroxysteroid-dehydrogenase/C4-decarboxylase activities, and act as key enzymes in C-4 demethylation in sterol biosynthesis. The leading model for the plant sterol biosynthesis pathway, suggested by Sonawane et al. (2016), consists of two branches producing cholesterol derivatives and phytosterols, respectively, with 3βHSD1 and 3βHSD2 acting in two demethylation steps of each branch (Figure S7) (Sonawane et al., 2016). A BlastP search identified nine 3βHSD enzymes in tomato, of which one (Solyc01g073640, referred to as both

GAME25 and 3βHSD1) has been shown *in vitro* to convert dehydro-type steroidal glycoalkaloids (SGAs) to dihydro-type SGAs (Sonawane et al., 2018; Lee et al., 2019).

The *hcr1* mutant shows a reduction in sterol content and modified sterol profile

To further investigate the potential link between HCR1 and the sterol biosynthesis pathway, bulk sterol levels were measured in leaves and fruit pericarp at three developmental stages by gas chromatography-mass spectrometry (GC-MS) (Figure 6 and Table S1). Leaves from *hcr1* showed similar sterol profiles to those of M82 during vegetative growth. Strikingly, the conjugated sterol fraction, including sterol glucosides (SGs) and acylated sterol glucosides (ASGs), in contrast to the free sterol fraction, were dominant in all measured tissues, accounting for more than 98% of total sterols (Figure 6). This predominance of conjugated sterols has been documented in several *Solanum* species as well as in oat (*Avena sativa*), in contrast to most plant species; for instance, conjugated sterols account for only about 20% of total leaf sterols in *Arabidopsis* (Furt et al., 2011, Wewer, 2011). However, the total sterol content of the *hcr1* pericarp was reduced to 84-89% of wild-type levels at 15 DAP, mature green, and red ripe stages; a difference that was statistically significant in all three stages (Figure 6). Similarly, the conjugated sterols (particularly sitosterol and stigmasterol) were dominant in the tomato fruit pericarp in all three stages and accounted for more than 90% of total sterols (Figure 6, Figure S6), which was consistent with previous findings (Whitaker et al., 1988, 1991 and 2008).

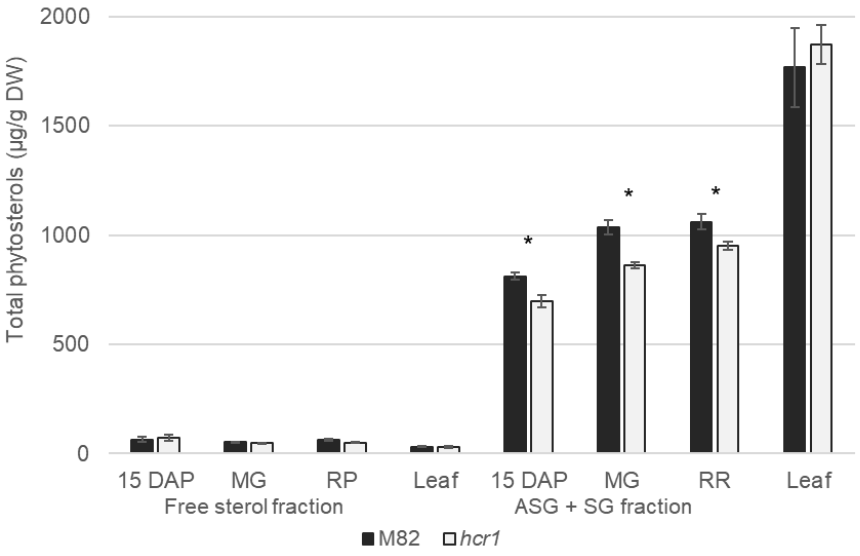

Figure 6. The sterol profile of fruit pericarps and leaves in M82 and *hcr1*. Total free sterols and total steryl glucosides are shown on the left and the right, respectively. (Mean ± SD of N = 3. * P < 0.01 by two-tailed t-test). Data collected by YH.

In addition to measuring total sterol content, individual sterols (campesterol, stigmasterol, sitosterol, cycloartenol, and cholesterol) were also measured. In the free sterol fraction, significant reductions in stigmasterol, sitosterol, and total sterols were observed in the red ripe *hcr1* fruit compared to M82, as well as in sitosterol in the leaves (Figure S6a). In addition, stigmasterol and sitosterol levels were reduced in the mutant SG + ASG fraction in all three fruit developmental stages measured (Figure S6b).

The *hcr1* mutant exhibits reduced cellulose levels in the fruit pericarp.

Several studies have suggested that structural sterols may be involved in cellulose biosynthesis (Peng et al., 2002; Schrick et al., 2004; Bessueille et al., 2009; Deng et al., 2016; Niu et al., 2019), although the mechanistic basis for this is not known. To examine the potential association between sterols and cellulose biosynthesis in the *hcr1* mutant, the crystalline cellulose content in the pericarp of *hcr1* and wild type fruit at the mature green (MG) and red ripe (RR) stage was

measured. The results showed that the crystalline cellulose levels in cell wall extracts of *hcr1* pericarp were reduced to 69% and 86% of that of the wild type, respectively (Figure 7a), suggesting cellulose deficiency during fruit growth. In contrast, the uronic acid levels, used as a measure of homogalacturonan pectin, of the *hcr1* fruit pericarp, though slightly reduced, was not significantly different from the wild type control at either stage (Figure 7b). Further, quantification of the cell wall matrix sugars revealed an over 6-fold increase in matrix glucose in the *hcr1* pericarp in comparison to M82 at the mature green stage (Figure 7c).

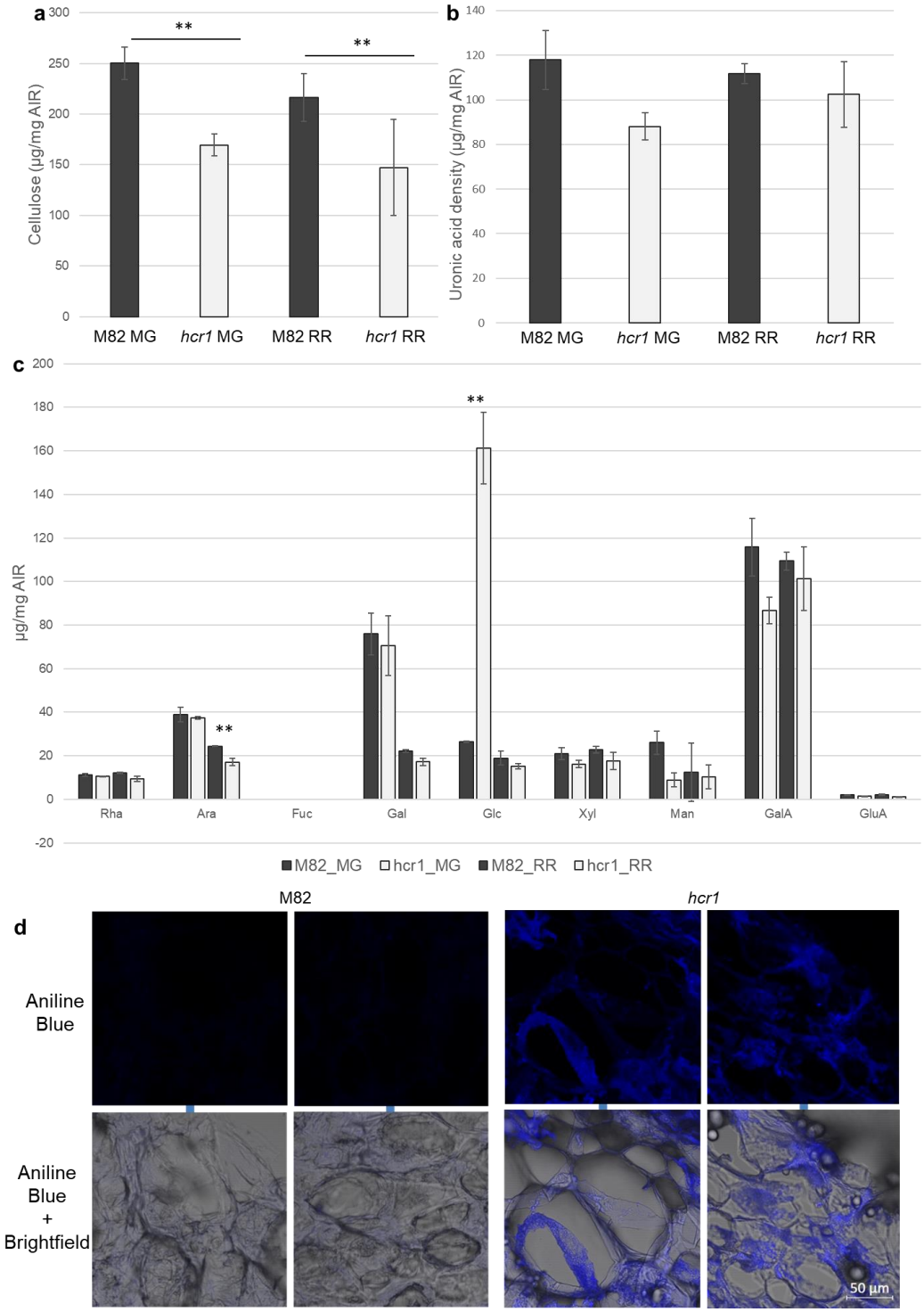

Figure 7. Analyses pertaining to cellulose biosynthesis in *hcr1*. (a) Cellulose density in M82 and hcr1 pericarp as measured by Updegraff. * indicates significance according to paired t-test ($p<.005$). (b) Uronic acid content of *hcr1* and M82 fruit pericarp as measured by Dionex. Paired t-tests identified no significant differences ($p<.05$). (c) Monosaccharide density in M82 and *hcr1* pericarp as measured by Dionex. * indicates significance according to paired t-test ($p<.05$). (d)

Confocal microscope images showing accumulation of callose in *hcr1* pericarp**.** Two representative images of each M82 and *hcr1* pericarps showing the aniline blue fluorescence channel (top row) and the aniline blue + TPMT merged channels (bottom row). Aniline blue staining around the cells is apparent in *hcr1* but barely discernable in M82. 50μm scale bar applies to all images.

Confocal microscopy imaging of pericarp stained with aniline blue to assess callose accumulation revealed a much higher affinity for the stain in the pericarp cells of *hcr1* than in M82, suggesting that this glucose accumulation in the mutant may represent callose, a polysaccharide known to be deposited between the plasma membrane and cell wall as reinforcement in response to wounding (Figure 7d) (Stone and Clarke, 1992). That the callose may be serving as a temporary cell wall to compensate for a cellulose deficiency during the rapid expansion phase of fruit development is consistent with the observed lack of heightened matrix glucose level in the red ripe fruit (Figure 7c).

DISCUSSION

The causal relations of the phenotypes on *hcr1* fruit

The rapid expansion of a tomato fruit requires an efficient coordination of tissue and cuticle synthesis during expansion. This study highlights the complexity of that process, and the severe consequences in terms of loss of surface integrity when that coordination fails. It also exemplifies the use of fruit as a system to study epidermal surface formation, as the phenotypes were very apparent in fruit but not in growing vegetative epidermal tissues, which may be under somewhat lower mechanical stress.

We observed essentially no differences between the ovaries of hcr1 and wild type prior to pollination at 0 DAP, however, by 3 DAP, several traits, including pericarp thickness, weight ratio of pericarp to inner tissue and the number of pericarp cell layers differed and (Figure 3d-g)

although a brown discoloration of the surface of some fruit, indicative of necrosis, was noticeable (Figure 1b). By 6 DAP, the average size of the parenchyma cells of the *hcr1* pericarp was significantly smaller than that of the control (Figure 3g) and discoloration was prevalent in most fruit, together with visible cracking on the surface of some fruit (Figure 1b). By this developmental time point, disordered epidermal cells with thickened wall cells were observed in pericarp cross sections (Figure 2a).

Other than the severe cracking, the most striking phenotype of the *hcr1* fruit was the absence of a fully developed pericarp (Figure 3a), which reflects a major impairment in both pericarp cell expansion and cell division. Interestingly, no major phenotypes were observed in other parts of the plant in this regard and the only other plant phenotype was the appearance of mild necrosis on some leaves. A reasonable hypothesis is that the *hcr1* mutation impairs cell division and expansion specifically in the pericarp and so as the fruit expand, the biomechanical stresses imposed on the outer pericarp tissues result in rupture and cracking. The cracking is first apparent as microfissures, detectable with scanning electron microscopy (SEM), which are associated with the early discoloration and necrosis, and these later develop into the major cracks, triggering tissue suberization.

Sterols are important for early fruit development.

Sterols are essential lipid components of cell membranes that provide stability to the phospholipid bilayer and play a critical role in maintaining membrane integrity and function. They may directly or indirectly modulate the activity of integral membrane proteins, including enzymes, ion channels, and signal transduction components (Schaller, 2003, 2004; Boutte and

Grebe, 2009; Valitova et al., 2016; Levental and Lyman, 2023). Plant sterols are also the precursors of the brassinosteroid (BR) hormones and so have considerable influence on a wide range of plant physiological processes (Asami et al., 2005; Wang et al., 2006; Li, 2010; Manghwar et al., 2022). Characterization of mutants with altered sterol profiles or genetic manipulation of sterol-related genes in *Arabidopsis thaliana* has revealed pleiotropic roles for sterols in plant growth and development. These include patterning of organs (e.g. embryo, vein, shoot, and root), seed development, cell expansion/elongation, cell polarity and proliferation, reactive oxygen species (ROS) regulation, cellulose biosynthesis, root hair initiation, and hormone signaling (Diener et al., 2000; Jang et al., 2000; Schrick et al., 2000, 2004; Carland et al., 2002, 2010; Peng et al., 2002; Souter et al., 2002, 2004; Willemsen et al., 2003; Men et al., 2008; Pose and Botella, 2009; Ovecka et al., 2010; Kim et al., 2012; Shimada et al., 2021). However, the molecular mechanisms underlying the specific phenotypes observed in many sterol-deficient mutants remain obscure and molecular downstream targets of sterols are largely unknown.

A common phenotype noted in many sterol synthetic mutants is dwarfism, which is thought to be caused by an inhibition of cell expansion and division (Schrick et al., 2000, 2004; Pose et al., 2009; Carland et al., 2010; Deng et al., 2016; Niu et al., 2019). BRs, derived from campesterol, are involved in numerous plant developmental processes, such as cell expansion and elongation, cell division, and cell wall regeneration (Clouse and Sasse 1998; Cano-Delgado et al., 2004; Nemhauser et al., 2004, Manghwar et al., 2022). However, the dwarfed phenotype of most sterol biosynthetic mutants cannot be rescued by exogenous BR treatment, indicating that structural sterol molecules themselves are crucial for cell expansion and division (Fujioka and Yokota,

2003; Schaller, 2003; Carland et al., 2010). Expression analysis demonstrated that exogenous application of both typical (sitosterol and stigmasterol) and atypical (e.g. 8, 14-diene sterols) sterols can activate the expression of genes involved in cell expansion and division, while sterol biosynthetic genes are regulated by several growth-promoting hormones, including BRs and auxin (He et al., 2003). This suggests the existence of a signaling crosstalk among sterols, hormones and the genes involved in cell growth; however, knowledge of the regulatory role of sterols in transcriptional regulation of cell growth-related genes is still extremely limited.

Various studies have indicated that sterols are involved in cellulose biosynthesis. As plant cell expansion and division require coordinated biosynthesis and restructuring of the cellulose-rich cell wall, perturbations in sterol biosynthesis may adversely affect cell wall formation and thus impair cell division and expansion (Rose and Bennett, 1999). In a comparative study of three sterol mutants, it was found that the *fackel*, *hydra1* and *smt1/cph* mutants shared similar cellular ultrastructural features, such as incomplete cell walls, aberrant wall thickenings and ectopic callose or lignin deposits, despite distinct variations in their sterol profiles. In addition, all three mutants exhibited a cellulose deficiency in the seedling cell walls, but normal levels of pectins and neutral sugars (rhamnose, fucose, arabinose, xylose, mannose, galactose), leading the authors to speculate that sterols are involved in cellulose synthesis (Schrick et al., 2004). This conclusion is shared by studies of cotton fiber cell elongation that have found that inducing changes to the sterol profile both exogenously and via overexpression of sterol biosynthesis genes suppresses cellulose production (Deng et al., 2016 and Niu et al., 2019). The mechanism by which this occurs, however, is unknown. Though Peng et al. (2002) reported that a cellulose synthase (Ces)A may initiate glucan polymerization using sitosterol-β-glucoside (SG) as a primer

(Peng et al., 2002), this model could not adequately explain the causal relations between sterol-deficiency and cellulose deficiency in some sterol mutants, as the primer role of SG may be easily fulfilled by residual levels of steryl glycosides (DeBolt et al., 2009).

A present hypothesis linking sterols to cellulose biosynthesis pertains to membrane raft-like domains of the plant plasma membrane (PM), the structure, composition, and possible functions of which have been studied in recent decades (Bessueille et al., 2009; Mongrand et al., 2010; Carmona-Salazar et al., 2011; Levantal et al., 2020). Sterols and sphingolipids are enriched in these raft-like plasma membrane domains and the self-associating properties of these two types of lipids are considered the main driving force for the formation of stable membrane domains (Silvius, 2005). It was reported that detergent-resistant membranes (DRMs) isolated from the PM of hybrid aspen contain key wall polysaccharide synthases, including callose synthase and cellulose synthases, with more than 70% of the total glucan synthase activities in the PM associated with this sterol-enriched DRM fraction (Bessueille et al., 2009). These results further support the possible involvement of structural sterols in cellulose biosynthesis. In addition, proteomic analyses have indicated that a high proportion of other proteins, such as ABCB19, OsRac1, and the REMORIN protein are associated with the DRM fraction, prompting speculation that DRMs may be involved in various physiological processes such as signaling, immunity, environmental stress responses etc. (Morel et al., 2006; Fujiwara, et al., 2009; Titapiwatanakun et al., 2009; Sezgin et al., 2017). Although detergent-resistant membranes do not explicitly define functional membrane rafts in plants (Boutte and Grebe, 2009; Tanner et al., 2011), such research has considerably increased our knowledge of the role of sterols in plant growth and development.

The high expression of the *HCR1* gene in the very early stages of M82 fruit development reflects a large demand for sterols in rapid cell expansion and division and indicates the importance of sterols for tomato early fruit development. In the *hcr1* mutant, on the other hand, it was noticed that several important phenotypic abnormalities emerged as early as 3 DAP, which coincides with the peak expression period (3-4 DAP) of the *HCR1* gene. This suggests that the phenotype may result from sterol deficiency due to the inactivity of 3β-HSD2 (*HCR1*) during this period (3-6 DAP). It is worth noting that the sterol profiling analysis was performed in the pericarp samples of 15 DAP or older fruit, since it requires a substantial volume of tissue; therefore, the status of sterol deficiency in the early developmental stage of *hcr1* fruit is not reflected in these data. That active synthesis of sterols is required during early tomato fruit development to meet the increasing demand for membranes as cells expand and divide is consistent with a previous work that has shown inhibited tomato expansion when 3-hydroxy-3-methylglutaryl-coenzyme A reductase (HMGR, a sterol precursor) is inhibited *in vivo* (Narita and Gruissem, 1989).

Evidence that sterols influence cellulose synthesis in *hcr1* fruit

Cellulose is the dominant structural component of plant cell walls. However, despite considerable progress made over past decades, many fundamental questions remain pertaining to the mechanisms, regulation, and modulation of cellulose synthesis and how these vary in response to environmental and developmental cues (Mutwil et al., 2008; Polko and Kieber, 2019).

As mentioned previously, studies of plants with altered sterol profiles (Schrick et al., 2004, Deng et al., 2016, Niu et al., 2019) and biochemical association of cellulose synthase activity with

sterol rich plasma membrane extracts (Bessueille et al., 2009) provide indirect evidence that sterols are important for cellulose synthesis. The crystalline cellulose content in the pericarp of *hcr1* fruit at 12 DAP or the mature green stage was only about 65-70% of that in wild type, which is a similar reduction to that reported for the three sterol-deficient *Arabidopsis* mutants (Schrick, et al., 2004). This suggests a possible causal relationship between sterol deficiency in the *hcr1* fruit and the reduction in crystalline cellulose, which could in turn lead to an inhibition of cell expansion/division, impaired pericarp development, and fruit cracking. Unlike in the *fk*, *hyd1* and *smt1/cph* mutants, the levels of bulk sterols in the pericarp of the *hcr1* mutant was only 11-16% less than those of wild type, possibly due to the activity of 3β-HSD family isozymes, though the reduction of crystalline cellulose content in the pericarp of *hcr1* fruit was substantial.

In addition to the overall sterol deficiency observed, the change of individual sterol abundances and their relative proportions in the mutant may disrupt cellulose biosynthesis. Both free sterols and glycosylated sterols are known to be important determinants of the structure and properties of cell membranes, and a series of studies indicate that the ratio of free sterols to glycosylated sterols in cell membranes is crucial for normal plant development and defense responses (DeBolt et al., 2009; Choi et al., 2014; Pook et al., 2017; Singh et al., 2016; Mishra et al., 2013; Saema et al., 2016; Pandey et al., 2014; Li et al., 2021). In the present work, the relative proportion of the ASG + SG fraction was reduced with respect to the free sterol fraction, the former of which is likely to be of elevated importance in tomato where it is predominant among total sterols (Chavez et al., 2023).

An *experiment* involving virus induced gene silencing (VIGS) of 3βHSD2 in tomato by Sonawane et al. (2016) similarly found significant reductions in several phytosterols, as well as in sterols from the cholesterol branch of the plant sterol biosynthesis pathway (Figure S7): they reported a reduction in α-tomatine in VIGS tomato leaves and green fruit, esculeoside B in red fruit, and reduced cholesterol, campesterol, sitosterol, isofucosterol, and Δ^7 avenosterol in leaves (Sonawane et al., 2016). Since the authors did not report a cracking phenotype in their fruit, we speculate that the VIGS knockout they used, in contrast to *hcr1* and CRISPR knockout lines was not as effective as suppressing gene expression and failed to fully provoke the phenotype. We also note that the genetic background in the VIGS experiments was MicroTom, as opposed to M82 in the present study, which may have lower levels of biomechanical strain in its fruit.

Further, the sterol profiles of the *fk*, *hyd1*, and *smt1/cph* mutants were marked by accumulation of abnormal sterols not measured in the present analysis, such as $\Delta^{8,14}$ sterols and an unknown stigmasta-monoen-3b-ol (Schrick, et al., 2004). Similarly, in an *experiment* involving VIGS of 3βHSD, 4-carboxysterol, an atypical sterol derivative which accounts for 2-3% of the total sterol content was detected in infected *Nicotiana benthamiana* plants (Rahier et al., 2006, 2011). Hence, we cannot rule out the possibility that some of the *hcr1* phenotypes are associated with the accumulation of abnormal sterols due to the reduced enzymatic activities of 3βHSD.

According to the hypothesized requirement of structural sterol molecules for the formation of the lipid raft microdomain that is the site of cellulose biosynthesis, we hypothesize that these disruptions in the normal sterol profile may be inhibiting the optimal function of the cellulose synthase complex, ultimately resulting in the distinct fruit cracking phenotype. Future studies

may investigate this by fluorescent-tagging cellulose synthases to observe whether their movement through the membrane is hindered in sterol mutants. Elucidating the precise character of this inhibition may shed light on the mechanism and requirements of cellulose biosynthesis.

MATERIALS AND METHODS

Plant materials

Seeds of *hcr1* mutant were obtained from the 'Genes that Make Tomatoes' EMS mutagenesis collection (Menda et al., 2004). Tomato plants were grown in the greenhouse at Cornell University, Ithaca, New York, under 16 hours of light and 8 hours of dark, using standard practices. Due to the low self-pollination rate of *hcr1* under greenhouse conditions, the flowers of *hcr1* and M82 were hand-pollinated and tagged. Fruit from mutant and wild type plants were harvested at the appropriate number of days after pollination (DAP). For the mature green (MG) stage, fruit were collected when they reached full size, but were still green and the red ripe (RR) stage corresponded to fruit 4-5 days after the color break.

Microscopy

For structural analyses of the fruit pericarp, fruit tissue was fixed and embedded in paraffin as described by Jackson (1992) and 6 μm paraffin sections of fruit pericarp were prepared. Sudan IV, Toluidine Blue and Neutral Red staining were conducted as described in Buda et al. (2009). For estimating cell size and the number of pericarp cell layers, paraffin sections were stained with Toluidine Blue and 10 or more sections were counted, as described in Vrebalov et al. (2009). The size of the parenchyma cells was estimated by counting cell numbers within a

certain area using ImageJ software (http://rsbweb.nih.gov/ij/) and 8 or more sections were measured each sample.

Genetic mapping of *HCR1*

An F_2 mapping population was generated by crossing the *hcr1* mutant with the wild tomato species *Solanum pimpinellifolium* (accession LA1589), and then harvesting F_2 self-pollinated seeds from F_1 progenies. Genomic DNA was extracted from young leaves of seedlings according to the method described by Fulton *et al*. (1995). Ninety-four plants of the *hcr1* F_2 population were phenotyped (using fruit cracking as the identifying trait), and then genotyped with 51 genetic markers that are distributed across the 12 chromosomes with an interval of about 10-30cM. Genotype and phenotype data were analyzed by Qgene 4.0.

Plasmid constructions and plant transformation

A binary vector pCAMBIA1305.1 was used as the basis of the β-glucuronidase (GUS) reporter (Jefferson et al., 1987) and complementation constructs. All PCRs were performed by Bio-Rad iProof^{tm} High-Fidelity PCR kit. For the native promoter complementation construction, a 3.1kb DNA fragment located upstream of *HCR1* coding region was amplified from M82 genomic DNA using gene specific primers (Forward: 5'-CCTTTAGTCTCAGGGCACA TGAA-3' and Reverse: 5'-TTCGTAGCGGATGAGC ATTTCGAC-3'). The native promoter was cloned into the *Pst I* and *BstE II* sites of pCAMBIA1305.1 vector. The coding region of *HCR1* was amplified from cDNA of M82 using gene specific primers (Forward: 5'-CAGTCGTCTTAAGCCAATGAGTGAA TGATGCTGCACG-3' and Reverse: 5'-CAGTCGTggttaccCCAATGAGTGAATGATG CTGCACG-3'); and then was subcloned into the

vector described above at *BstE II* site. For the 35S promoter construct, the coding DNA of *HCR1* gene was amplified using gene specific primers (Forward: 5'-ACTGCagatctCATGGGTGAAGAAAAATGGT GTGTGGTGAC-3' and Reverse: 5'-ACCTCAcacgtg GGATGTTCTCCCATCAATGC TAGACCA-3'); and then was cloned into the pCAMBIA 1305.1 vector at *Bgl II* and *Pml I* site. For the GUS reporter expression construct, the native promoter was amplified using the gene specific primers (Forward: 5'-CCTTTAGTCTCAGGGCACATGAA-3' and Reverse: 5'-ACGCCAGccatggTGCCAAGAGATTGAGATTCTTCAAGG-3'), then was cloned into the pCAMBIA 1305.1 vector by replacing the CaMV35S promoter fragment using *Pst I* and *Nco I* for the enzyme digestion. For the CRISPR construct, CRISPR sgRNA targets were identified using the CRISPR-PLANT tool (https://www.genome.arizona.edu/crispr/CRISPRsearch.html) and off-target identification tool Cas-OFFinder (http://www.rgenome.net/cas-offinder/). The CRISPR construct was made according to Belhaj et al. (2013). The pICH86966::AtU6p::sgRNA_PDS construct (Addgene #46966) was used to amplify sgRNA1 and 2 (sgRNA1 5'-tgtggtctcaattGACATTCGGCTGGGGTACGACgttttagagctagaaatagcaag-3'; sgRNA2 5'- tgtggtctcaattGGGGCAGCATTTAACGAAATAgttttagagctagaaatagcaag-3'; with universal reverse 5'-tgtggtctcaAGCGTAATGCCAACTTTGTAC-3') to be inserted into the pICH47751 (addgene # 48002) and pICH47761 (addgene #48003) vectors, respectively, in a level 1 cloning reaction including the pICSL01009::AtU6p (addgene #46968) vector. The resulting two pICH47751::sgRNA1 and pICH47761::sgRNA2 vectors were then used in a level 2 cloning with the pICH47732_NPTII (addgene 3 #51144), pICH47742_35S:Cas9 (addgene #49771), pICH41780 (addgene #48019) and pICSL4723 (addgene #86173) vectors.

The two complementation constructs were transformed into *hcr1* mutant plants by *Agrobacterium*-mediated transformation (Van Eck et al., 2006) using the plant transformation facility in UC Davis. The GUS construct and CRISPR construct were each transformed into M82 plants by the *Agrobacterium*-mediated method (Van Eck et al., 2006; http://irc.igd.cornell.edu/Protocols/Tomatotransform.html) in the plant transformation facility at the Boyce Thompson Institute or Plant Research, Cornell University. CRISPR mutations were verified with PCR amplification of gDNA and subsequent sequencing.

Sterol profiling

Tomato leaf tissue (without petioles) was harvested from the leaves at the third node counting from the top of each plant when flower buds in the first inflorescence were still small. Fruit pericarp samples were collected from 3 different stages: 15 DAP, MG, and RR. Samples were flash frozen in liquid nitrogen and lyophilized in FreeZone Freeze Dry System (Labconco, Model: 77520) for 24 hours and then stored in plastic screw-cap tubes at -80°C until being subjected to lipid extraction.

Extraction was performed as described by Wewer et al. (2011) with minor modifications. A total of 1g of material was used for lipid extraction with 15 ml of chloroform/methanol (2:1). For each extract, a phase separation was effected by addition of 5 ml of 0.145 M NaCl solution. The sample was vortexed and centrifuged for 2 min at 5000 g. The non-polar fraction containing free sterols was removed with a pipette. Two additional extractions of chloroform/methanol (2:1) were performed and the organic phases combined, and the solvent was evaporated under N_2 gas. The polar fraction containing non-free sterols were separated by TLC in acetone:toluene:water

(91:30:8) and the lipids isolated from the silica plates with chloroform:methanol (2:1). This fraction was hydrolyzed in 1 ml 1 N methanolic HCl at 90°C for 30 min. After the addition of 1 ml of 0.154 M NaCl solution, the hydrolyzed sterols were extracted with 1 ml of hexane. Sterols were derivatized with 100 µl N-methyl-N-(trimethylsilyl)-trifluoroacetamide (MSTFA) and analyzed by comparison with authentic standards using GC-MS (GC: 6890 series, HP and Mass Selective detector: Agilent, Model: 5973).

RNA isolation, cDNA synthesis and quantitative PCR analysis

Pericarp tissue from three biological replicates for each stage were harvested, flash-frozen in liquid nitrogen, and stored at –80°C. For un-pollinated ovaries/fruit (at 0 DAP), whole fruit were sampled as it was difficult to separate ovary wall/pericarp from adjacent tissues. Total RNA was isolated from frozen tissue (10-80 mg) using an RNeasy mini kit (Qiagen) and on-column DNase digestion was performed with the RNase-free DNase set (Qiagen), following the manufacturer's instructions. A total of 3 µg of total RNA was used for cDNA synthesis with SuperScript III reverse transcriptase and oligo (dT) primers (Invitrogen), according to the manufacturer's instructions.

Quantitative PCR experiments were performed using 7900HT Real-Time PCR System (Applied Biosystems) with 384-well block module. Twenty microliter qPCR mixtures, prepared with 10 µl 2× HotStart-IT SYBR Green qPCR Master Mix (Affymetrix, Santa Clara, CA, USA), 6 µl 30-fold diluted cDNA and 4 µl other reaction components (Primers: 0.5 µl each, ROX passive reference dye: 0.4 µl and water: 2.6 µl) were loaded into each well of a 384-well plate. To estimate PCR amplification efficiency, calibration dilution experiments were performed in the

same plate using a dilution series (10-fold dilution from10× to 10^5× as well as a blank and a 30× dilution) from the cDNA mixture which was mixed with the same volume of cDNA from each sample. The default thermal cycling condition for standard 384-well plate was applied for all qPCR runs (95°C for 10 min, 40 circles: 95°C for 15 seconds, 60°C for 60 seconds), and a dsDNA high-resolution melt curve analysis was performed.

The sequences of oligonucleotide primers are listed in Table S2. Specificity of the products was determined by product sequencing, gel electrophoresis and dissociation/melting analysis. qPCR data were analyzed using SDS2.1 software (Applied Biosystems). A mean normalized expression of genes was calculated using Q-Gene software (http://www.gene-quantification.de/download.html) in Microsoft Excel. The *ribosomal protein L2* (*RPL2*) gene (Yeats et al., 2010) was used as a constitutive control in all gene expression experiments.

GUS histochemical staining

Pericarp sections were cut by hand from fresh tissues and fixed in cooled 80% acetone for about 30 minutes. GUS histochemical staining was performed according to Jefferson et al. (1987).

Cellulose and uronic acids analysis

The procedure for lignocellulosics cell wall isolation and the acid hydrolysis of the cell walls for cellulose measurement was performed as described by Foster et al. (2010). The amount of glucose hydrolyzed from crystalline cellulose was measured using the colorimetric PAHBAH (p-hydroxybenzoic acid hydrazide) assay (Blakeney and Mutton, 1980), in which the absorbance

values were measured by Multiskan EX Microplate Photometer (Thermo Electron Corporation) with 405nm filter.

Cell wall polysaccharide analysis via high-performance anion-exchange chromatography with pulsed amperometric detection (HPAEC-PAD) of paired samples was performed as described by Yeats et al. (2016) using a Dionex ICS-5000 HPAEC-PAD system (Thermo Fisher Scientific, Fisher Scientific, model: ICS-5000+ SYSTEM) and Chromeleon 7 software (Thermo Fisher Scientific). Average values represent 2 technical replicates of tissue pooled from 3+ fruit.

Aniline blue staining and confocal microscopy

Blocks of outer pericarp from MG fruit were fixed and cryosectioned to 12 μm as previously described (Buda et al., 2009). The sections were bound to Histobond slides (VWR) by heating at 100°C for 3 minutes. The embedding medium was rinsed off with deionized water, and the sections were stained with 0.1% aniline blue A967 for 30 minutes before rinsing and mounting with water. Samples were imaged with an LSM 710 confocal microscope (Zeiss) using a 40X water-immersion objective, a 405nm excitation wavelength and 475-525nm filter. Images were processed using Zen software (Zeiss) and are false-colored.

ACCESSION NUMBERS

F_2 mapping population was generated by crossing the *hcr1* mutant with the wild tomato species *Solanum pimpinellifolium*, accession LA1589.

CHAPTER 2:

Investigation of a Transcuticular Trichome Pore Sealing Phenomenon that Inhibits Fruit Water Loss using Wild Tomato *Solanum quitoense* as a Model System

INTRODUCTION

Nonstomatal water loss through the hydrophobic cuticle contributes significantly to overall water loss in all land plants, especially in desiccating conditions when stomata have closed (Santrucek et al., 2004). In this case, the cuticle, which covers the surfaces of all aerial organs, is the major barrier against transpirational water loss from the apoplast of epidermal cells. Cuticles are composed of a structurally complex lipidic polyester, termed cutin, as well as polysaccharides and various soluble compounds that are referred to collectively as waxes (Schreiber, 2010; Yeats and Rose, 2013), and their permeance varies over 500-fold across plant species (Riederer and Schreiber, 2001).

Many compositional features underlying the variation in cuticle permeance remain to be resolved. Cuticular waxes are believed to play a critical role in restricting transpiration but while there is no correlation between total wax levels and cuticular permeance across, or within, species, the wax compositional profile may influence permeance (Jordan et al., 1984; Schreiber and Riederer, 1996; Riederer and Schreiber, 2001; Schreiber 2010; Parsons et al., 2013). For instance, it has been found that the ratio of aliphatic compounds to triterpenoids is a key factor affecting permeability, with a higher proportion of triterpenoids correlating with increased permeability, though this only explains a small portion of the total variation (Vogg et al., 2004; Leide et al., 2011; Buschhaus and Jetter, 2012; Parsons et al., 2013; Jetter and Riederer, 2016).

Since tomato fruit cuticles lack stomata and can be readily isolated, they provide a valuable model for studying cuticle structure, composition, and attributes (Martin and Rose, 2014). In an assessment of fruit cuticular permeance across a germplasm diversity panel of tomato (*Solanum lycopersicum*) accessions it was also found that in addition to waxes, the permeance correlated strongly on the abundance of microscopic polar pores across the cuticle (Fich et al., 2020). These microscopic pores were found to be associated with trichomes and were exposed when trichomes were dislodged as previously reported (Blanke, 1986; Paul and Srivastava, 2006; Fich et al., 2020). Furthermore, staining of the pore areas with Toluidine Blue revealed that they have the capacity to become sealed, an adaptation with implications for water retention and relevant to open research questions regarding cuticle structure and remodeling (Fich et al., 2020; Berhin et al., 2022). The hypothesis guiding the present work is that the deposition of a cuticle or cell wall polymer, such as cutin, lignin, suberin, or cellulose, at the trichome pore site is the cause of this sealing phenomenon.

Trichomes are epidermal cell outgrowths that exist on the aerial organs of most seed plants. They have diverse single cellular and multicellular morphologies and a range of functions, including acting as a protective barrier against herbivores, pathogen attacks, ultraviolet irradiation, and excess transpiration (Wang et al., 2021). Though most research has focused on the trichomes on leaves and stems, they are also found on the fruits of many plant species, and some research attention has been given to them for their involvement in preventing pathogen infection (Yan et al, 2020; Watts and Kariyat, 2021; Shen et al., 2023). In the recent tomato study identifying trichome-associated pores as major routes for water loss, sealing of these pores was observed in

fruit of the M82 commercial cultivar after trichomes were removed when the fruit was midway through the expansion phase (Fich et al., 2020). While more conspicuous trichomes exist on some fruit, such as peach (*Prunus persica*), kiwi (*Actinidia deliciosa***)**, raspberry (*Rubus idaeus*), chestnut rose (*Rosa roxburghii*), cucumber (*Cucumis sativus*), and eggplant (*Solanum melongena*) (Wang et al., 2019; Xue et al., 2019), the trichomes on commercial tomato cultivars are sparse, microscopic, and diverse in type and size, making the sealing process difficult to quantify and investigate. Among tomatoes, the South American wild relative *Solanum quitoense* (common name: naranijlla) displays large, abundant, and uniformly spaced trichomes on the fruit surface, and here we used this expedient model for studying the sealing process.

RESULTS

Trichome morphology varies across tomato species and organs

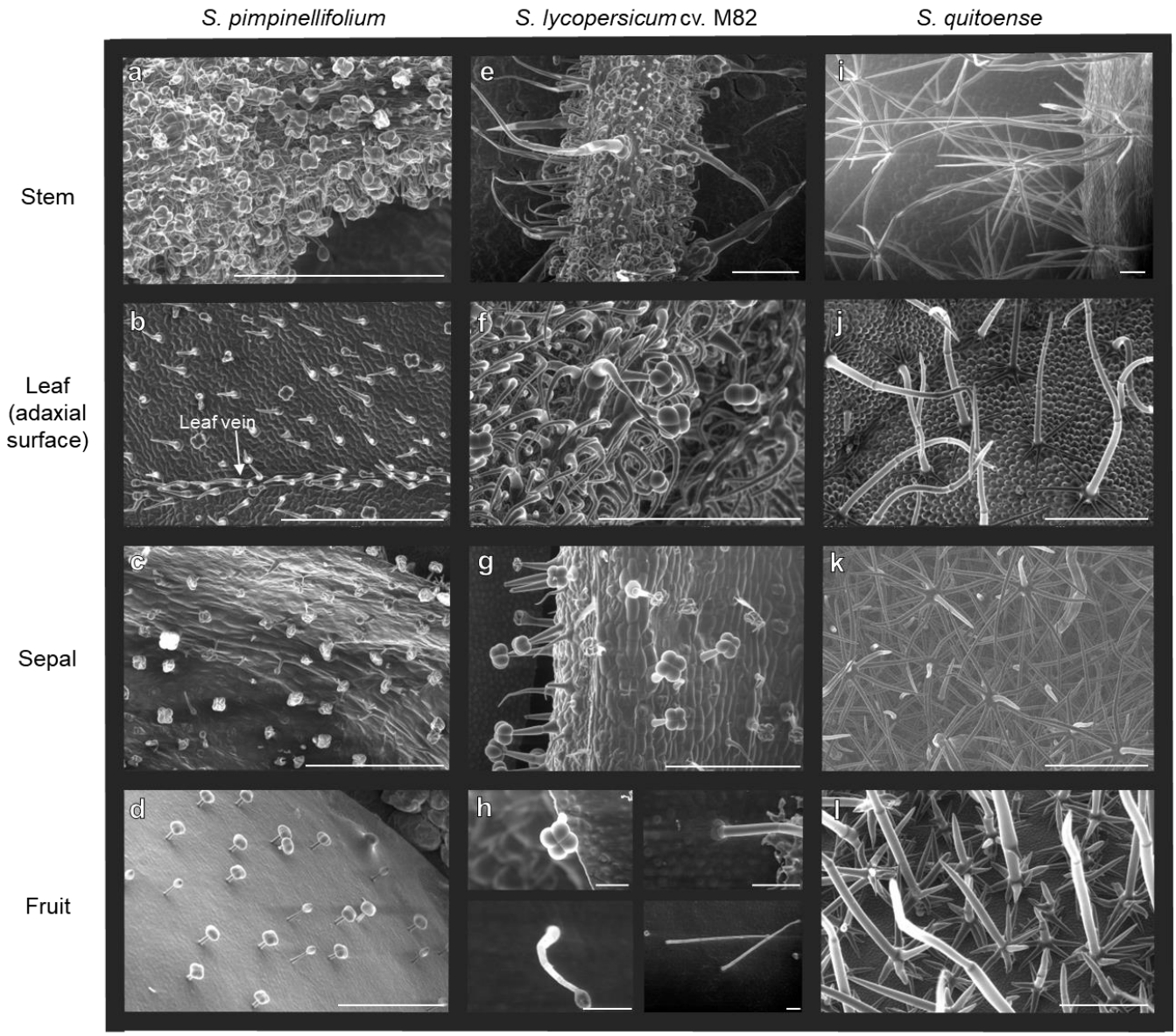

Figure 1. Scanning electron micrographs showing diverse trichome types on the stems, leaves, sepals, and fruit of (a-d) *S. pimpinellifolium*, (e-h) *S. lycopersicum* cv. M82, and (i-l) *S. quitoense.* Scale bars: (a-g; i-l) = 500 µm, (h) = 100 µm.

A variety of single- and multi-cellular trichome types are present on the stems, leaves, sepals, and fruit of *S. lycopersicum* cv. M82 (Figure 1e-h). Though a system for categorizing *Solanum*

trichome types was established by Luckwill (1943) and used over past decades, it has recently been criticized for failing to include many trichome types and for proposing a glandular/non-glandular binary that does not reflect the complexity of trichome morphologies observed in the family (Simmons and Gur, 2005; Watts and Kariyat, 2021). Instead, and consistent with our data, Watts and Kariyat documented at least seven types of trichomes present on the adaxial surface of *S. lycopersicum* leaves at densities ranging from "very rare" to 5.04 trichomes per square millimeter (Figure 1e-h) (2021). We observed that trichomes were especially dense on stems and along leaf veins.

We also imaged trichome types on various structures of *S. pimpinellifolium*, a pre-domestication wild relative of modern cultivated tomato (Figure 1a-d) and observed three trichome types, with morphologies consistent with those documented in other nightshades by Watts and Kariyat: 1) glandular hairs with a quadricellular globular head and a single stalk cell; 2) an attenuate basilatus glandular hair with a small glandular tip; and 3) attenuate *non-glandular* hairs with jointed multicellular stalks (2021). The third type was absent on the fruit. Thus, not only was M82 observed to have a greater diversity of trichomes types, but a higher density on the leaves. Further, the largest trichomes types present on M82 were absent on *S. pimpinellifolium* (Figure 1b,f). This suggests that an increase in trichome diversity, size, and density across all organs occurred during tomato domestication.

For further analysis we selected the wild tomato relative *S. quitoense*, which has abundant trichomes clearly visible to the naked eye (Figure 1i-l). Another trichome-dense tomato wild relative, *S. pennellii*, was considered for the study, but found to be less suitable for our

experiments as the sticky exudate released from the trichomes inhibited their removal. In contrast to *S. lycopersicum* and *S. pimpinellifolium, S. quitoense* has only one trichome type on each organ. The *S. quitoense* leaves, sepals, and fruit each have slight variations of a trichome morphology called "porrect-stellate", consisting of star-like, radial branching at the point of attachment to the cuticle and a single central projecting branch (Figure 1j-l). Porrect-stellate trichomes with various branch numbers and proportions have been documented on other members of the Solanaceae, including *eggplant*, forest bitterberry (*Solanum anguivi*), lance-leaved nightshade (*Solanum lanceifolium*)*, and p*otato tree (*Solanum grandiflorum*) (Watts and Kariyat, 2021). On the *S. quitoense* stem, trichomes have a similar but inverted shape in which the radial projections occur at the distal end of the trichome with respect to the stem (Figure 1i). These highly branched structures could reflect interesting environmental adaptations; perhaps to maximize organ cover and windbreak while minimizing sites of attachment.

Dense, abundant *S. quitoense* trichomes provide a model system for studying trichome pore sealing

Several features of *S. lycopersicum* trichomes make them unfit for systematic study of the sealing phenomenon: principally, their diversity in morphology and size makes it difficult to distinguish trichome pore sealing from variation in the size of the pores left by different trichomes. Further, they are microscopic and easily broken by slight contact, making it difficult to determine whether any given trichome was removed intentionally at an experimental time point or by abrasion during fruit development, which often occurs during standard plant care.

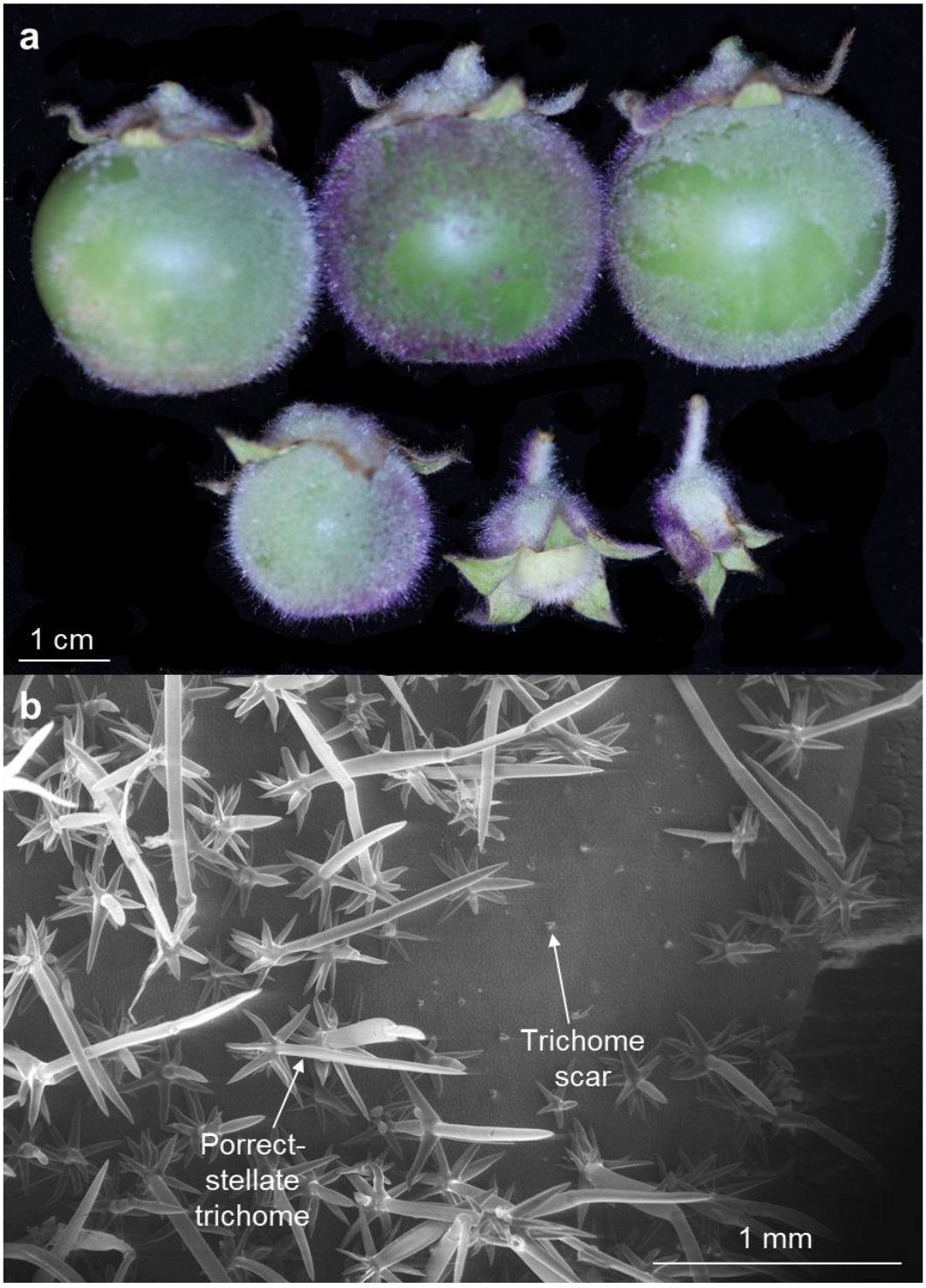

Figure 2. Features of wild tomato relative *S. quitoense*. a) Photos of fruit throughout development densely covered by large trichomes. Patches of exposed cuticle are apparent where trichomes have been removed by abrasion. b) Scanning electron micrograph showing the porrect-stellate morphology of the trichomes and the scars left behind when they are removed.

In contrast, the trichomes on *S. quitoense*, which are large, dense, and uniform, provide a far more expedient model for studying trichome sealing. The fruit are covered by a carpet of trichomes from the earliest stages of fruit development (Figure 2a) (Ramírez and Davenport, 2020), which can be easily removed by physical contact, and the patches of exposed cuticle left behind in their absence make it clear when trichomes have been accidentally disturbed by plant care. Scanning electron microscopy (SEM) imaging can also be used to show that when a patch of trichomes is removed, a uniform pattern of scars can be observed on the cuticle surface at the sites of their former attachment (Figure 2b). Because there is only one type of trichome present, the variation in the morphology of these scars is minimal and predictable, so changes in their appearance over time can be attributed to the sealing system.

Evapotranspiration experiments indicate that sealed trichome pores inhibit water loss across the cuticle

To assess whether trichome removal and exposure of the pore resulted in an increase in fruit water loss, whole *S. quitoense* ripe fruit were harvested and weighed at intervals after either having their trichomes removed or retained at the time of harvest (n=5-7 fruit). While fruit retaining trichomes lost 3.3% of their weight at harvest (Day 0) by Day 3, 8.6% by day 12, and 12.3% by day 25, fruit that had their trichomes removed at harvest had lost 5.4%, 14.2%, and 20.9% respectively, representing a statistically significant increase in whole fruit water loss at every time point measured (Figure 3a). This indicates that removing trichomes resulted in more water loss than if the trichomes remained attached to the fruit, despite any sealing of the pores that occurs within this 25-day period.

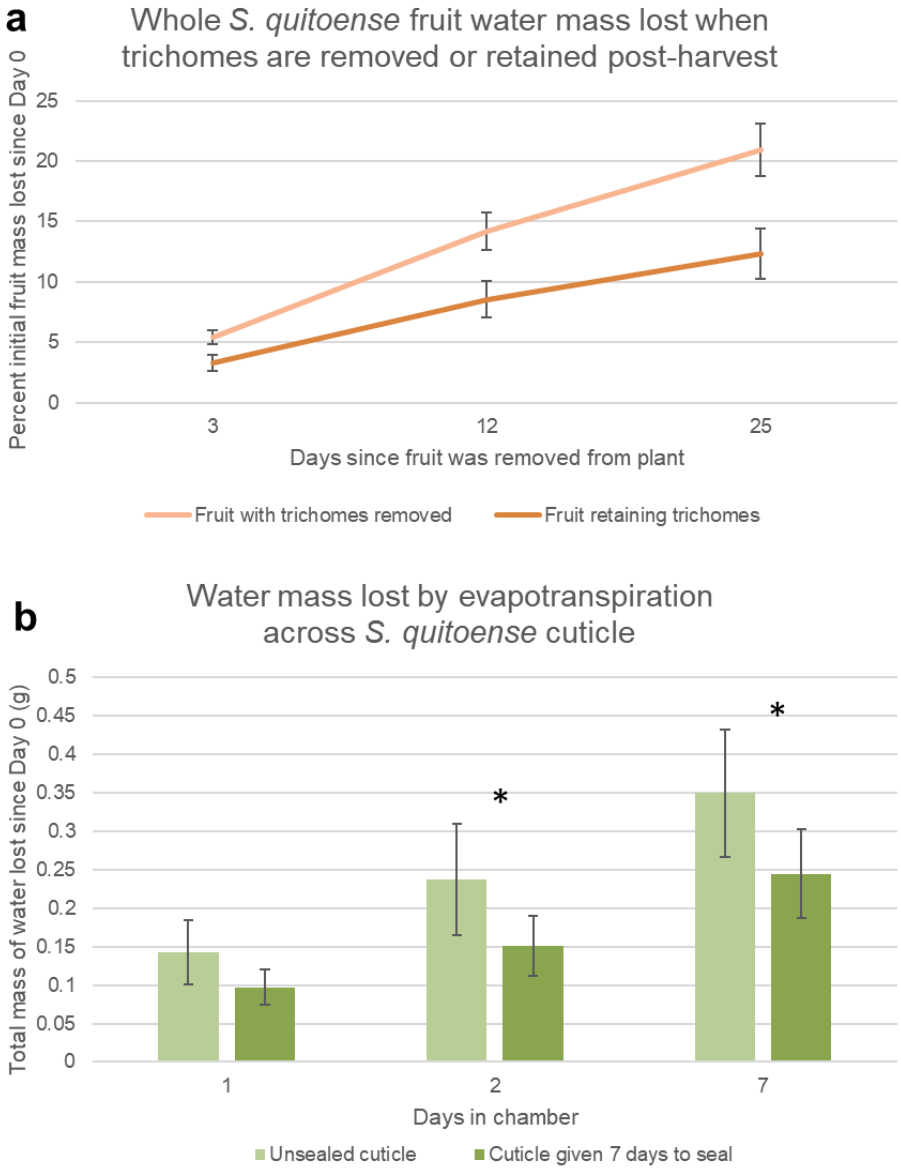

Figure 3. *S. quitoense* water loss experiment results

To examine the effect of the sealing of the pores on transcuticular water loss, an experiment was performed using a transpiration chamber system in which cuticles were secured in a water-containing chamber to act as a barrier to evaporation (Figure 4). The test groups included *S. quitoense* cuticles isolated by cellulase and pectinase digestion of the associated polysaccharide cell wall, which either had their trichomes removed at the time of harvest (Unsealed) or 7 days

prior to harvest to allow sealing time (Sealed). The experiment showed that the mass of water lost to evaporation through the cuticle was larger in the Unsealed fruit at the 1-, 2-, and 7-day timepoints measured, with the change being statistically significant at the 2- and 7-day timepoints (Figure 3b). This experiment confirmed that the sealing process has meaningful ramifications for the water retention capacity of the fruit.

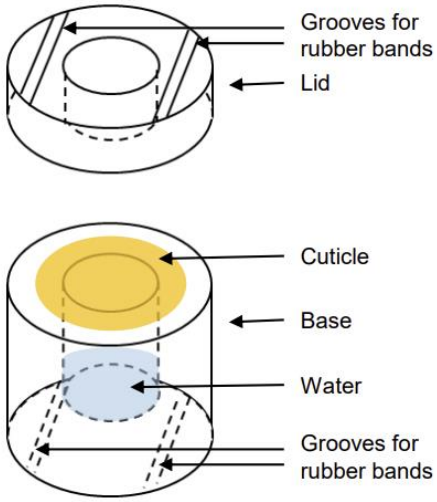

Figure 4. Schematic diagram of evaporation chamber system

The size of *S. quitoense* trichome pores decreases with sealing time, with the largest size change occurring within the first three days after trichome removal

A technique to identify trichome pores in *S. lycopersicum* via staining with the hydrophilic dye Toluidine Blue following trichome removal was established by Fich et al. (2020). Applied to *S. quitoense*, this method revealed a fruit surface covered in relatively large, uniform stained pores. To better understand the nature of the pore sealing process, staining was performed both immediately after trichome removal and 7 days after trichome removal (in both cases, staining was performed immediately after fruit harvest) (Figure 5a). Imaging of the stains and quantification using ImageJ software of many replicates (n=9-14 fruit) revealed that the number

of stained trichome pores was not reduced by this sealing time, but that the size of the stains was significantly reduced to an average of 58-66% of their initial size (Figure 5b-c), a decrease in pore size discernible by a dissecting microscope (Figure 5a). A time course experiment was undertaken to plot the average stain size over 9 days following trichome removal while the fruit was still attached to the plant. The experiment showed that that the size of the pores decreased rapidly over the first several days following exposure, nearing a plateau by Day 3 (Figure 4d). This data collectively suggested that the sealing response is relatively rapid and widespread among pores, and a scar is always retained, as opposed to restoring a smooth cuticle.

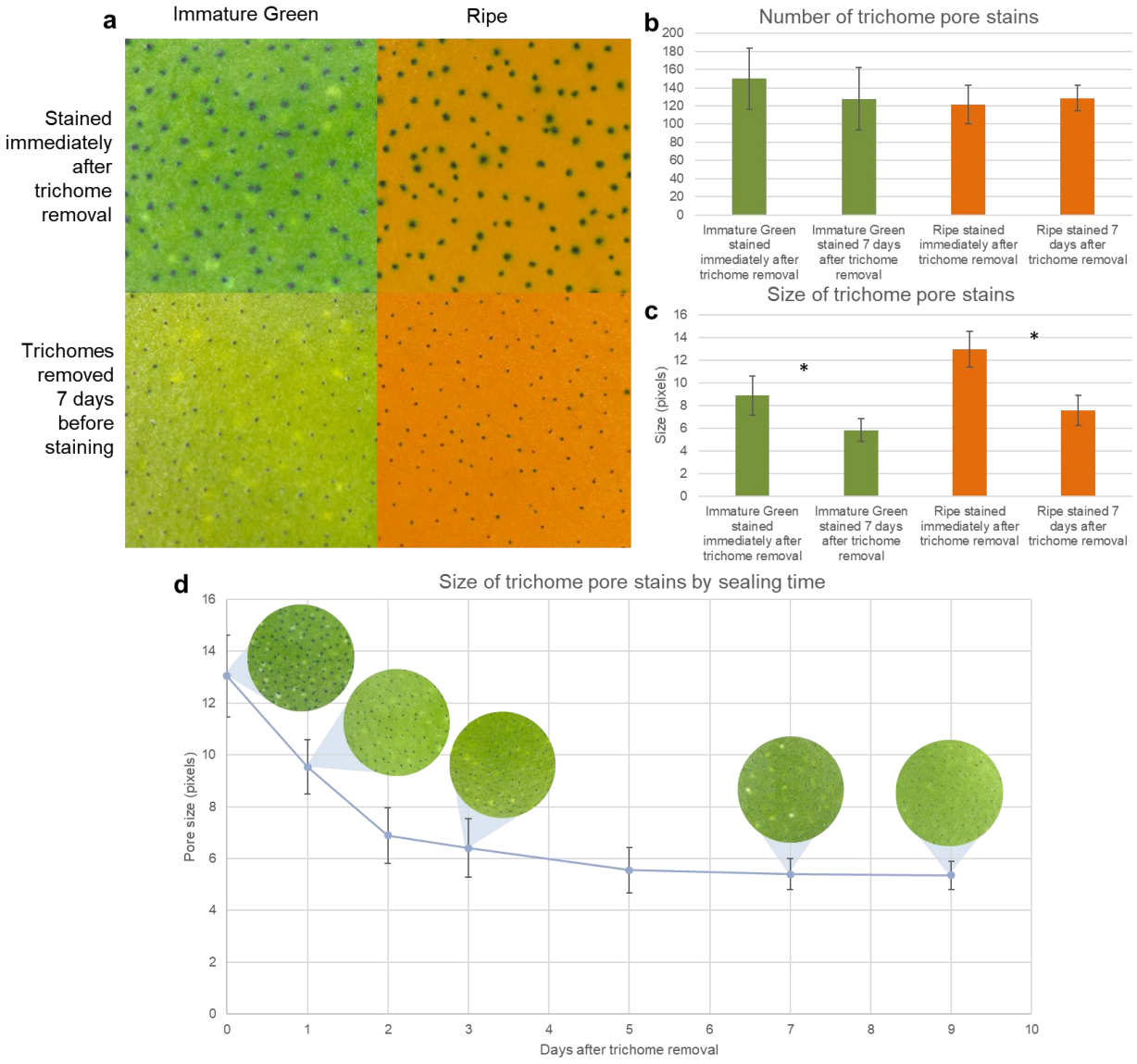

Figure 5. Images and data pertaining to the staining of *S. quitoense* trichome pores with Toluidine Blue. a) Cuticles stained with Toluidine Blue showing larger stains immediately after trichome removal. b-c) Graph bars represent mean of 9-14 biological replicates. Error bars indicate standard deviation. * indicates $p<.05$ by two-tailed T-test. d) Data points reflect the means of 3 biological replicates. Error bars indicate standard deviation.

Pore sealing limits the spread of Toluidine Blue through the cuticle

We next wanted to investigate anatomical changes that underly the reduction in pore size over time. Scanning electron microscopy of unsealed and 5-day sealed trichome pores was performed to analyze the change in surface morphology. The unsealed trichome pores consistently had large open cavities, clearly exposing the cell walls at the base of the removed trichome (Figure 6a). The pores that were allowed to seal for 5 days had variable appearance: some retained an open appearance, resembling the unsealed pores (Figure 6b), while a deposited material that was absent from the unsealed samples either fully or partially covered the cavities in the sealed samples. The identity of the deposited material was unidentifiable by SEM. As the Toluidine Blue quantification experiment indicated that a reduction in stain size occurs consistently across pores (as opposed to in some pores and not others) (Figure 5a-c), we concluded from this experiment that while there is sometimes evidence of pore sealing at the surface, the phenomenon causing the reduction in Toluidine Blue stain size likely occurs deeper in the cuticle profile.

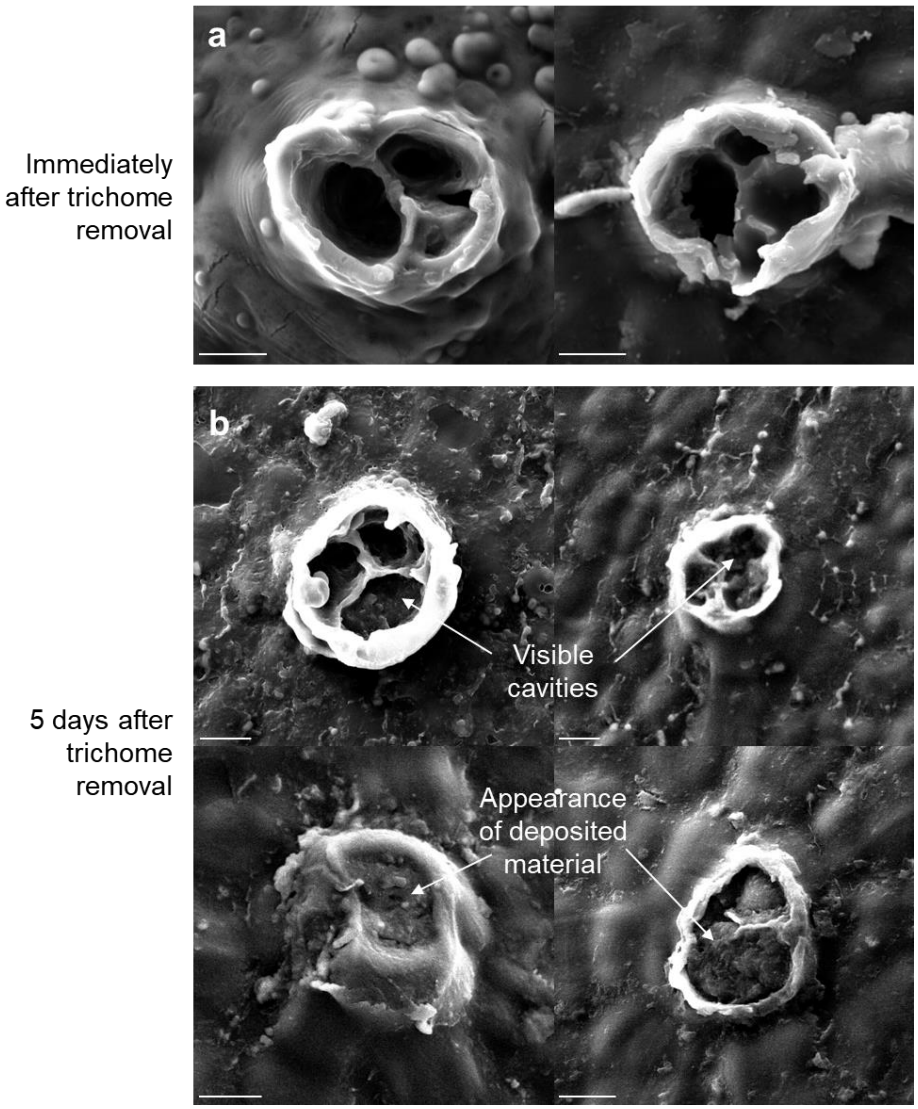

Figure 6. SEM images of trichome scars prepared a) immediately after removal and b) after 5 days of sealing time

To better understand the anatomical context of the Toluidine Blue stained areas – for instance, how deep the stain was permeating into the cuticle – we replicated the Toluidine Blue staining experiment and obtained cross section images. We observed that in the fruit with pores given time to seal, the stain remained confined to a diameter averaging approximately 35 micrometers near the fruit surface. However, in the fruit where pores were not given time to seal, the stain was

observed at a high concentration in the same area, but also was dispersed more diffusely in the surrounding area, surrounding several cells in either direction (Figure 7a). This width of the stained area averaged approximately 60 micrometers. We placed these measurements in the context of the SEM images, which also explained the basis for the decrease in Toluidine Blue stain size documented previously: in the sealed pores, the stain was confined to the area of the trichome scar itself, while in the unsealed samples, the larger stained areas reflected the seeping of the stain to the cells surrounding the pore, which is evidently visible through the cuticle (Figure 7b). The difference in Toluidine Blue spreading between the sealed and unsealed samples suggests that the sealing occurs via barrier formation in the cuticle in a sub-surface region at the base of the trichome scar (Figure 7a).

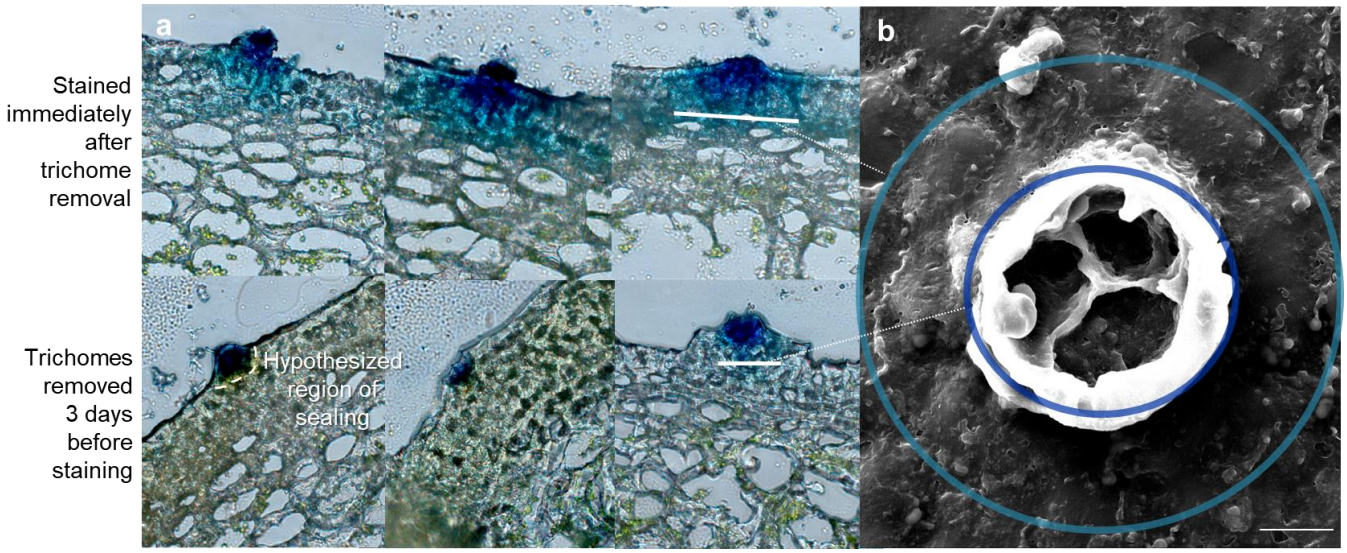

Figure 7. a) Light microscope images of Toluidine Blue stained unsealed (top row) and sealed (bottom row) trichome pores in cross section, and b) an SEM image for anatomical context

Sealing mechanism cannot be discerned by comparative confocal imaging with staining for major structural compounds

The Toluidine Blue-stained cross section experiment led to the hypothesis that there may be barrier material deposition below the surface of the cuticle, so this region was targeted using confocal imaging. *S. quitoense* trichome pore cross sections were stained with three stains to identify major compounds of the cuticle and cell wall likely to be involved in the sealing mechanism: Calcofluor White, which exhibits selective binding to cell walls composed of chitin, cellulose, and other beta-1,4-linked carbohydrates and is commonly used as a general cell wall stain; Fluorol Yellow, a suberin stain that also commonly binds cutin due to structural similarity; and Basic Fuchsin, which has been used as a lignin-specific stain in *Arabidopsis thaliana* and *Brachypodium distachyon* (Ursache et al., 2017).

Sealed trichome pores

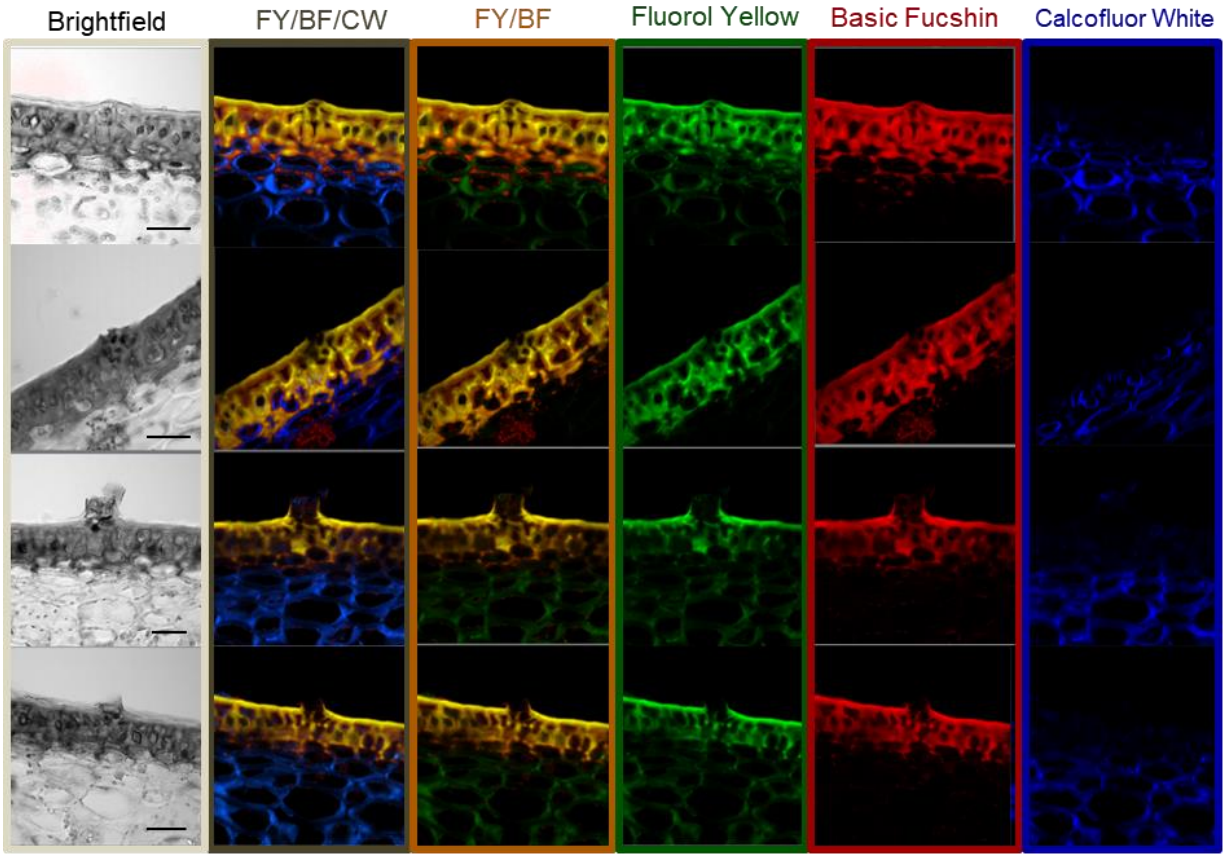

Unsealed trichome pores

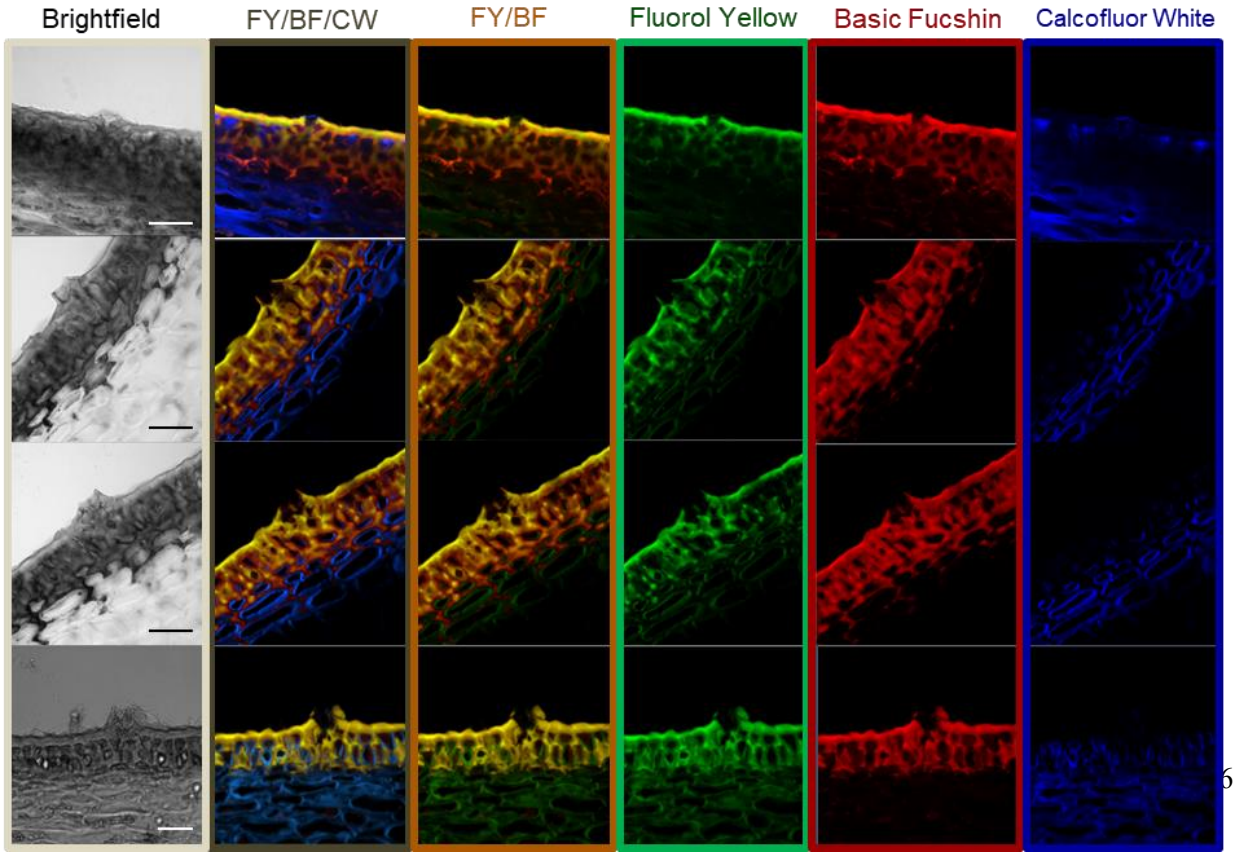

Figure 8. Confocal images of sealed and unsealed trichome pores, with various stain channels indicated. Scale bars = 30 micrometers.

An initial observation using these stains on *S. quitoense* was that there was significant overlap in the tissues stained by Fluorol Yellow and Basic Fuchsin, with both consistently staining the entire cuticle and some of the underlying cell walls, but with Fluorol Yellow staining cell walls deeper into the pericarp than Basic Fuchsin (Figure 8). This overlap and affinity for the cuticle suggests that the stains were not highly specific for suberin and lignin in *S. quitoense*, in contrast to their characterization in *Arabidopsis thaliana* roots (Yokoyama et al., 2007; Ursache et al., 2017). This lack of specificity is consistent with the high structural similarity between lignin, suberin, and cutin and the existence of phenolic polyesters with intermediate structure (Philippe et al., 2020).

Though many trichome pores were imaged (n>20), a consistent visual difference between the sealed and unsealed pores was not apparent (Figure 8). Z-stack images were analyzed to test several hypotheses about the possible appearance of sealing: we considered whether the sealing phenomenon might be visible as: 1) the lack of an opening at the surface of the trichome pore; 2) the lack of an evident vertical channel from the fruit surface through the cuticle profile; 3) depositions in the hypothesized sealing region; or 4) generally thickened cuticle architecture. However, none of these hypotheses was confirmed, as no distinct features were consistent across samples or between groups. The complex architecture of the *S. quitoense* cuticle is a limitation to attempts to understand the sealing process via imaging, as its thickness and texture obscure small

cavities and are problematic for distinguishing a potential sealing-related material deposition from typical variation in cuticle architecture.

DISCUSSION

This work highlights several important attributes of the trichome pore sealing system in *S. quitoense*. Removal of trichomes at harvest significantly increases fruit water loss, confirming that the trichome pores are significant routes of water loss, as in *S. lycopersicum*. However, isolated cuticles that have been allowed to seal prior to isolation allow less transcuticular water loss than those isolated immediately after trichome removal, indicating that pore sealing effectively inhibits this water loss through pores. Staining the cuticle with Toluidine Blue and imaging the surface revealed that the area of the pore stain gets measurably smaller with sealing time, plateauing at approximately 3 days. Viewing these stained pores at cross section, contextualized to SEM images, suggests that the sealing does not occur at the surface of the trichome scar, but rather along the base of the exposed cavity. Evidence of the sealing mechanism was not captured by confocal microscopy, possibly due to the complexity of the *S. quitoense* cuticle architecture and the lack of specificity of stains primarily characterized in *Arabidopsis*. This rules out, however, that the sealing mechanism involves a large (>10 micrometer) material deposit, as this would have been detectable.

It remains possible that the sealing mechanism involves a deposition of structural material such as cutin, lignin, suberin, cellulose, or a combination thereof, perhaps in a precise, targeted manner and small scale in response to specific routes of water loss. Cellulose may be the material least likely to be involved in the sealing response, as cellulose was digested in the

cuticle isolation process prior to the evaporation chamber experiment that showed that the sealed cuticles retain more water. However, it cannot be ruled out that trace cellulose remains following isolation and could contribute to this effect. It is also possible that the sealing simply reflects desiccation due to evaporation through the trichome pore, causing a dry apoplastic environment in which the Toluidine Blue does not spread effectively. However, this makes the observed decrease of water loss of the sealed fruit in evaporation chambers difficult to explain.

Several approaches may prove useful in better understanding this process. Most simply, a replication of the confocal imaging experiment on a higher-resolution microscope may identify depositions not yet detected. A high replicate number will be necessary to be certain that traits interpreted as causal are not singular events due to biological variation in cuticle architecture. To rule out that the phenomenon reflects desiccation in the apoplast, fruit could be submerged in water or a high-humidity environment during the sealing period and then stained. Further, an experiment using Fourier-transform infrared spectroscopy (FT-IR) probing over a sealed trichome pore may be an effective way to identify an enrichment in lipids or polysaccharides. However, a pilot experiment to that end using a Bruker Vertex V80V Vacuum FT-IR system showed that the *S. quitoense* cuticle is too thick (approximately 80 micrometers) for the required light transmission, posing a technical barrier to such a study. A more promising approach might be to characterize transcriptional responses to trichome removal: an experiment could involve laser-capture microdissection for isolation of epidermal cells before and after trichome removal and RNA sequencing to identify an upregulation of genes involved in, for instance, cutin biosynthesis or transport.

Importantly, this work was performed in *S. quitoense* because of its amenability to study, but it will be important to test whether these findings generalize to tomatoes of greater commercial interest, especially *S. lycopersicum*. Though the microscopic, sparse, and diverse trichomes on this species will be more difficult to quantify, many of the experiments described here can be readily repeated in M82, such as the water loss experiments. Imaging the trichome pores in cross section will require preparation of many slides, as the relative scarcity of the trichomes makes them difficult to capture. However, the M82 cuticle, which is thinner than that of *S. quitoense*, will be more amenable to FT-IR experiments.

MATERIALS AND METHODS

Plant material and growth conditions

S. quitoense plants were grown from 10 cm cuttings of a plant in the Cornell Botanic Garden collection. All plants were grown in Cornell Mix soil in 2-gallon pots in a green house in Ithaca, New York with 16-h daylength. Growers were careful to avoid disturbing trichomes during plant care. Most analyses studied mature green (MG) stage fruits, defined as those that have developed to the size of ripe fruit but have yet to show color change. In all cases, the amount of 'sealing time' reported (e.g., 2 days sealing time) refers to the period between removing trichomes by gently wiping the fruit surface with gloved finger and harvest, during which the fruit remained on the plant, otherwise undisturbed. After the sealing period, the fruit were harvested at the same time as their 'unsealed' counterparts, whose trichomes remained undisturbed until analysis.

Scanning electron microscopy

To image trichome pore scars, squares of outer pericarp approximately 5mm^2 were cut from freshly harvested fruit with a razor blade. They were mounted on SEM stubs using an adhesive sticker, immersed in liquid nitrogen, freeze-dried overnight, and sputter coated with gold-palladium, and imaged with a Hitachi 4500 scanning electron microscope at Cornell University.

As trichomes were too fragile to undergo the freeze-drying required for the above preparation method, a cryo-SEM system was used to image the intact trichomes on various tomato organs without drying. Small sections of tissue were cut with a razor blade, immersed in liquid nitrogen, mounted on the microscope stage with prongs, and imaged using a ThermoFisher Quattra FESEM at the Skidmore Microscopy Imaging Center (SMIC).

Toluidine Blue staining of fruit surfaces and cross sections

For Toluidine Blue staining of the fruit surface, whole fruits were submerged in 0.05% Toluidine Blue (Sigma 198161) in water for 15 hours. The fruit were then rinsed with deionized water, allowed to air dry for several minutes, and imaged with a Stemi 508 stereo microscope (Zeiss).

For Toluidine Blue staining of trichome pore cross sections, whole MG fruits were stained as described above and then blocks of outer pericarp were cut out, embedded, cryosectioned to 30 μm, and placed on Histobond slides (VWR) as previously described (Buda et al., 2009). These sections were not fixed to avoid dispersing the stain. The sections were imaged with an Axio Imager A1 microscope (Zeiss).

Quantification of pores

Following the Toluidine Blue staining and imaging of the fruit surface described above, the pores were quantified in number and area using the Fiji ImageJ software (imagej.nih.gov). Each image was cropped to show 4mm^2 of the fruit surface before importing to ImageJ. For each image, a series of edits were made to make the pores clearer for automated quantification: Enhance Contrast (Saturated pixels: 1%), Subtract Background (Rolling ball radius: 50.0 pixels), Image Type changed to 16-bit, Image Threshold adjusted such that the highlighted area matched the pores. The Analyze Particles function was then used (Size: 2-Infinity) to generate a count of pores and their average size in pixels.

Cuticle isolation

Discs of outer pericarp (diameter ~2cm) were cut from the fruit with a razor blade and incubated in a solution of cellulase (Sigma, catalog no. C2605; 0.013 dilution) and pectinase (Sigma, catalog no. P2611; 0.0023 dilution), containing 0.01% (w/v) sodium azide, at 42°C for multiple weeks, after which the digested tissue was washed off the cuticle with water. The discs were stored in water at room temperature.

Whole fruit water loss and transpiration chambers

To measure whole fruit water loss, MG fruit were removed from the plant and either had all trichomes removed or were left undisturbed according to their experimental group. The initial mass of each fruit was measured. Fruit was left at room temperature and weighed at intervals.

To measure water loss through the cuticle, isolated cuticles were mounted in a transpiration chamber system (Figure 4) at room temperature with monitoring to avoid large fluctuations in ambient temperature or humidity. Each chamber was weighed at intervals to measure water lost due to transpiration.

Staining and confocal microscopy of cross sections

Blocks of outer pericarp were cut from fruit with a razor blade, fixed, embedded, and cryosectioned to 15-30 μm as previously described (Buda et al., 2009). The sections were bound to Histobond slides (VWR) by heating at 100°C for 6 min and embedding medium was rinsed off gently with deionized water. Staining with Basic Fuchsin, Fluorol Yellow, and calcofluor white and mounting was performed following the "Triple staining of cell wall components" described by Ursache et al. (2017) without the optional tissue clearing steps. Confocal microscopy was conducted using the Zeiss LSM 710 confocal microscope using a 40X water-immersion objective at the Cornell BRC Imaging Facility (NIH S10RR025502). Excitation wavelengths for each stain were configured using the Zen Smart Setup feature. Z-stack images were captured at various interval lengths and analyzed using Zen and Imaris software.

APPENDIX

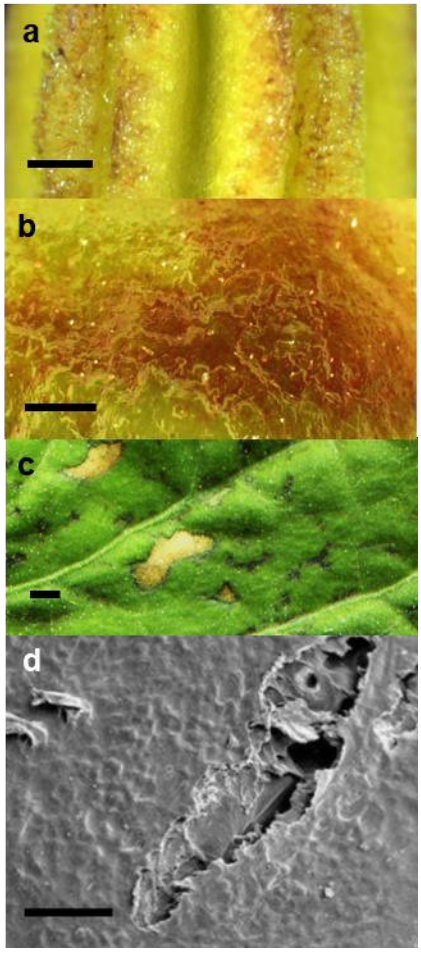

Supplemental Figure 1. Additional phenotypes of *hcr1* mutant.
(a) Enzymatic discoloration on anther surface of *hcr1* mutant.
(b) Discoloration phenotype of young *hcr1* fruit.
(c) Necrotic spots on a leaf of the *hcr1* mutant.
(d) SEM micrograph of cracks on *hcr1* fruit.
Scale bars: (a-b) = 500 µm, (c) = 2 mm, (d) = 50 µm.

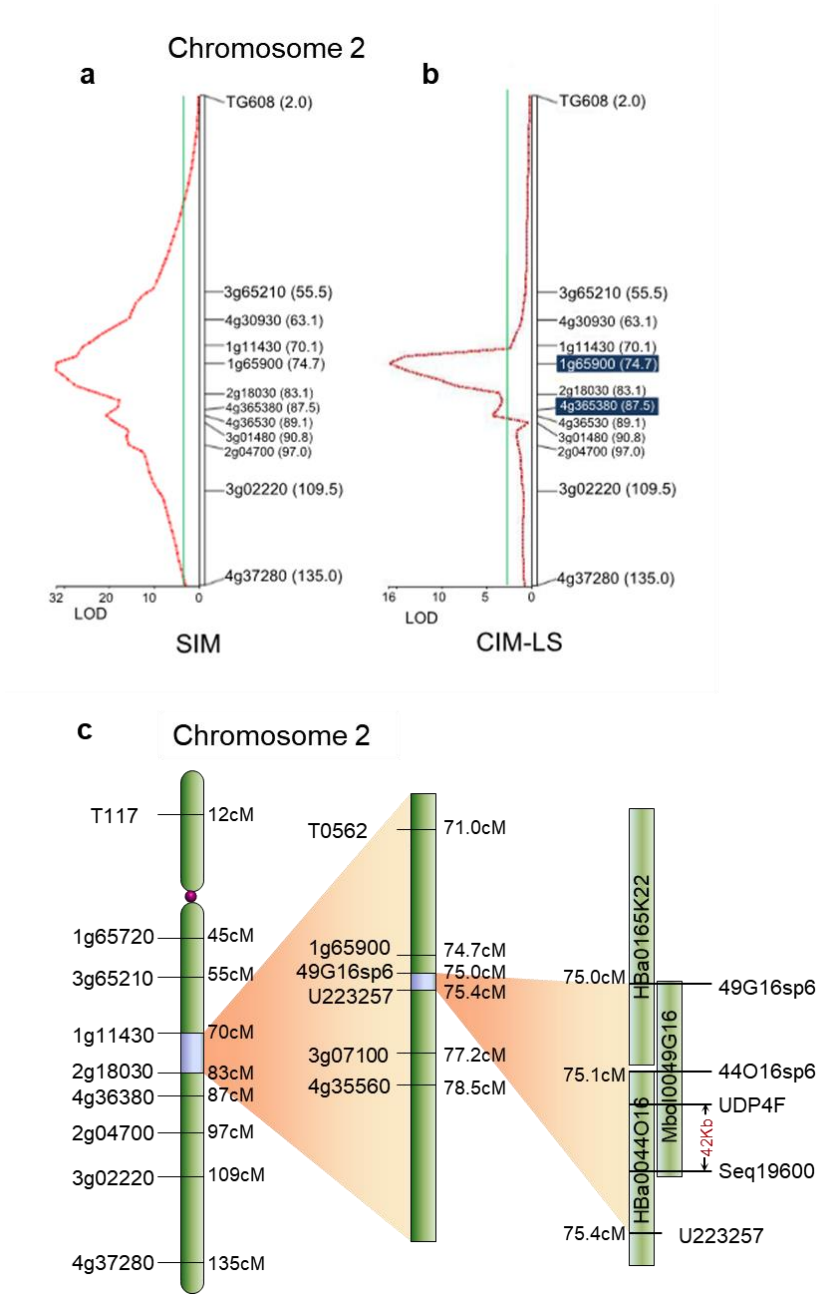

Supplemental Figure 2. QTL map of the hcr1 mapping population.
(a) QTL analysis using Simple Interval Mapping (SIM)
(b) QTL analysis using Composite Interval Mapping (CIM-LS) with cofactor marker (with blue background) selection. The red line indicates the value of log-likelihood ratio (LOD) and the green line indicates the LOD threshold (>3). The number in parentheses indicates the marker location in cM.
(c) Schematic diagram showing the mapping of *hcr1* to chromosome 2 between the marker Seq19600 and UDP4F.

Target	Forward Primer Sequence	Reverse Primer Sequence	PCR length (bp)
RPL2 Solyc10g006580	CAGCGGATGTGTGCTATGAT	GGGATGCTCCACTGGATTCA	154
3β-HSD1 (HCR1-1) Solyc02g081730	AGCGTACTTGGGATCATTTCACC	TCCCATCAATGCTAGACCA	140
3β-HSD1 (HCR1-2) Solyc02g081730	GCAAGTGACCAACTAGGATACGCACCT	ATCCTTTCCCGACCCGTGTTC	108
Polyphenol Oxidase F Solyc08g074630	AGCCTTCATGAGTTGGTGGCT	AGGCAGTAACGAGCTATCCAGC	124
Polyphenol Oxidase E Solyc08g074620	GTCTGCATGAGTTGGTGGCT	AGCATTAACACAACTAGAATCAGC	130
GDSL-motif lipase/hydrolase Solyc11g006250	GTAGCATGTTGTGGACAAGGACCA	TTTGCCCTCTAGATGGATGGAAC	122
SlCER6 Solyc02g085870	CCAGTGTTCATCCCAGAGATTGTC	GTCTGAGAGCTACACACGTT	171
Feruloyl-Coenzyme A Transferase Solyc03g097500	ACGGATTTCGGGTGGGGAGA	CTTCATAGCTGAAGCTGGCAGTCC	138
SlCESA1 Solyc08g061100	AGAGGTATGTGGCTTGGACTGTG	CCCCTTGTTCCTTCTCCCTGAGT	99
SlCESA6-like Solyc04g071650	CTGGGCTGTTCTCCTTGCATCC	ACCACATTGACCTCTTGCAGCA	99
SlCESA3 Solyc01g087210	GGACCAGATGTTCAGGCTTGTGG	TCACATGGATGACCTTCAGCT	95

Supplemental Table 1. PCR primers used for gene expression analysis.

Supplemental Figure 3. Confirmation of the HCR1 locus. Phenotypes of (a) *hcr1* EMS mutant, T0 transgenic lines transformed with (a) Native promoter :: HCR1 cDNA, (b) CaMV35S :: HCR1 cDNA, and (c) CRISPR constructs targeting HCR1.

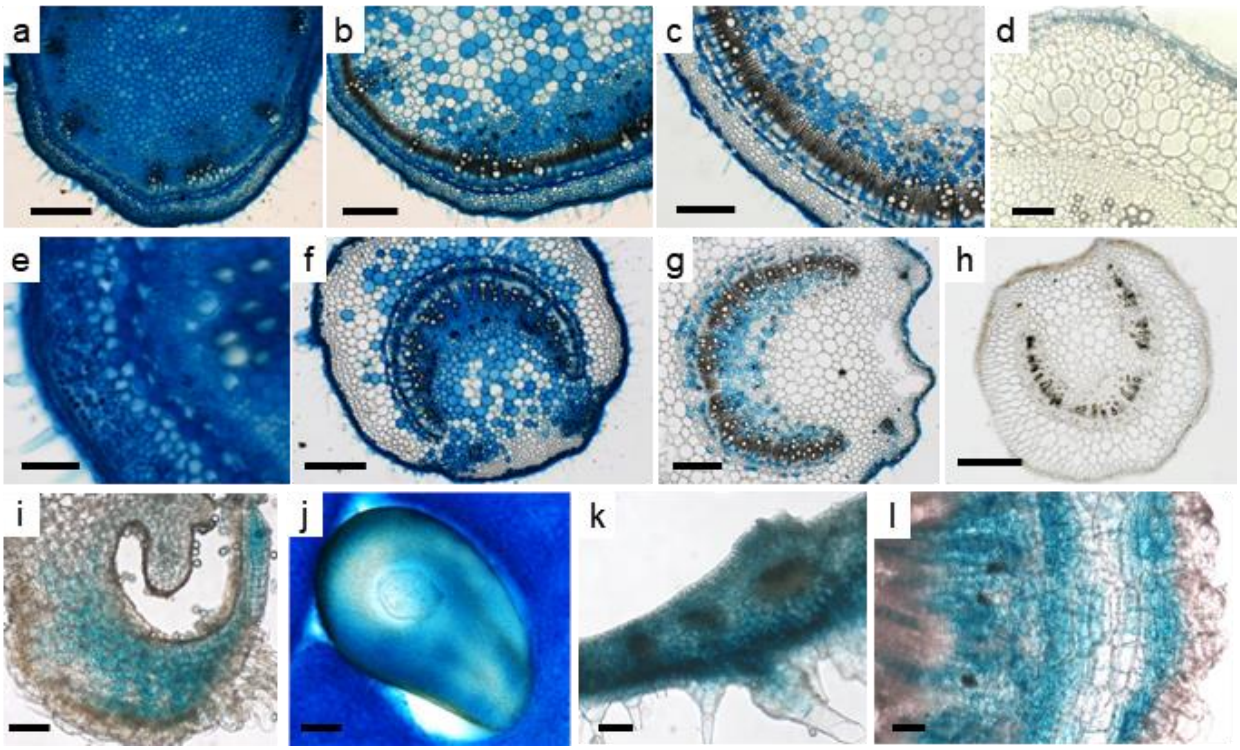

Supplemental Figure 4. Spatial and developmental expression analysis of *HCR1* gene using the GUS reporter system.

(a-d) GUS staining of cross sections of stems at different stages from younger (a) to older (d).
(e-h) GUS staining of cross sections of petioles at different stages from younger (e) to older (h).
(e-l) GUS staining in other tomato organs: anther (i), ovule (j), sepal (k) and root (l).
Scale bars (a, b, f-h) = 500 µm, (d, e, i-l) = 100 µm

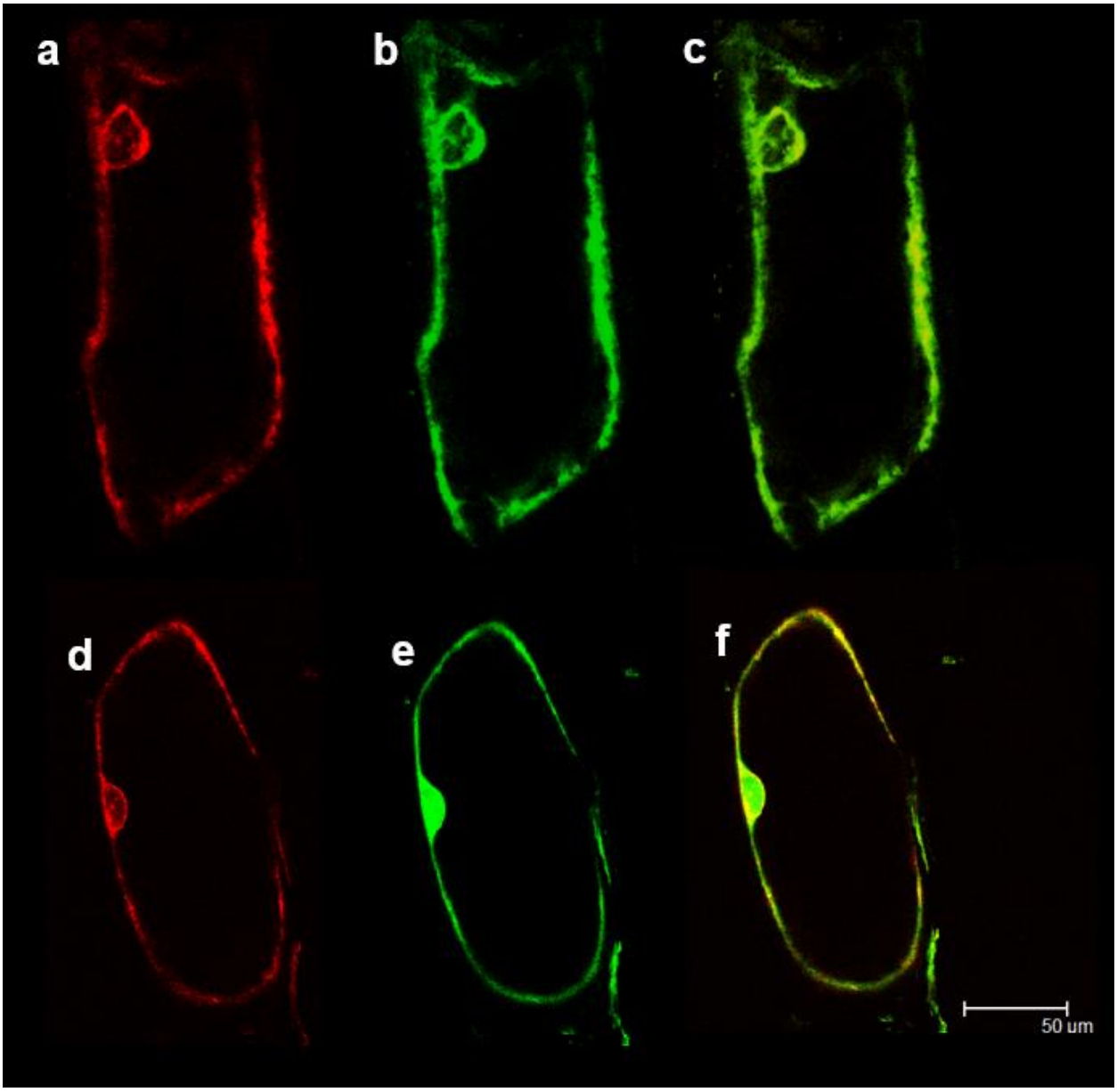

Supplemental Figure 5. Subcellular localization of HCR1. ER localization of HCR1=tdTOM protein (a) showed co-localization with GFP-ER marker (b), with the corresponding merged image (c). (d-f) Localization of a cytoplasmic GFP marker (d) was compared to that of HCR1-tdTOM (e), with the corresponding merged image (f).

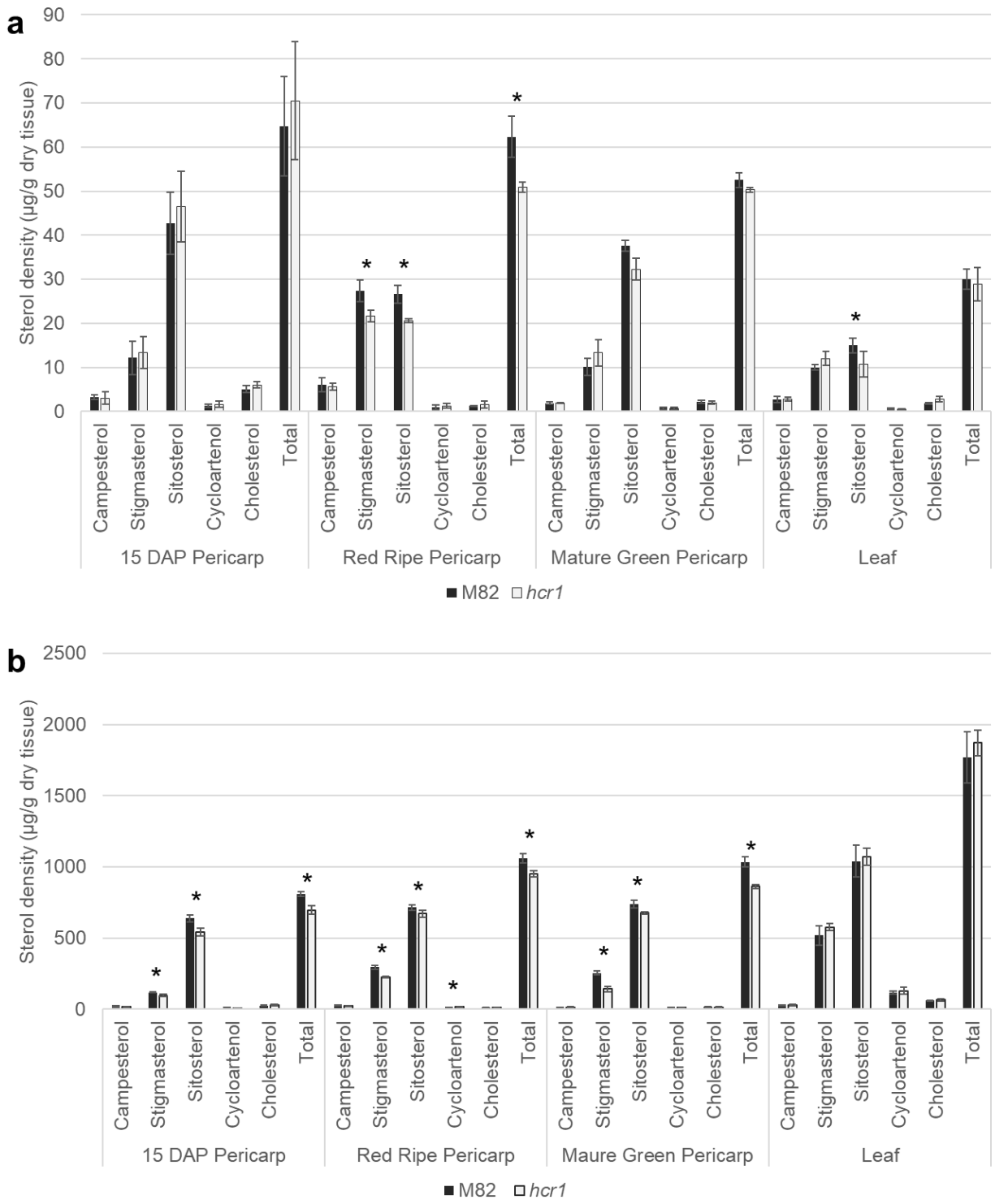

Supplemental Figure 6. Specific sterol profiles. Density of sterols in fruit pericarps and leaves in M82 and *hcr1* within (a) the free sterol fraction and (b) the steryl glycoside + acyl steryl glycoside fraction. (Mean ± SD of N = 3. * $P < 0.01$ by two-tailed t-test.)

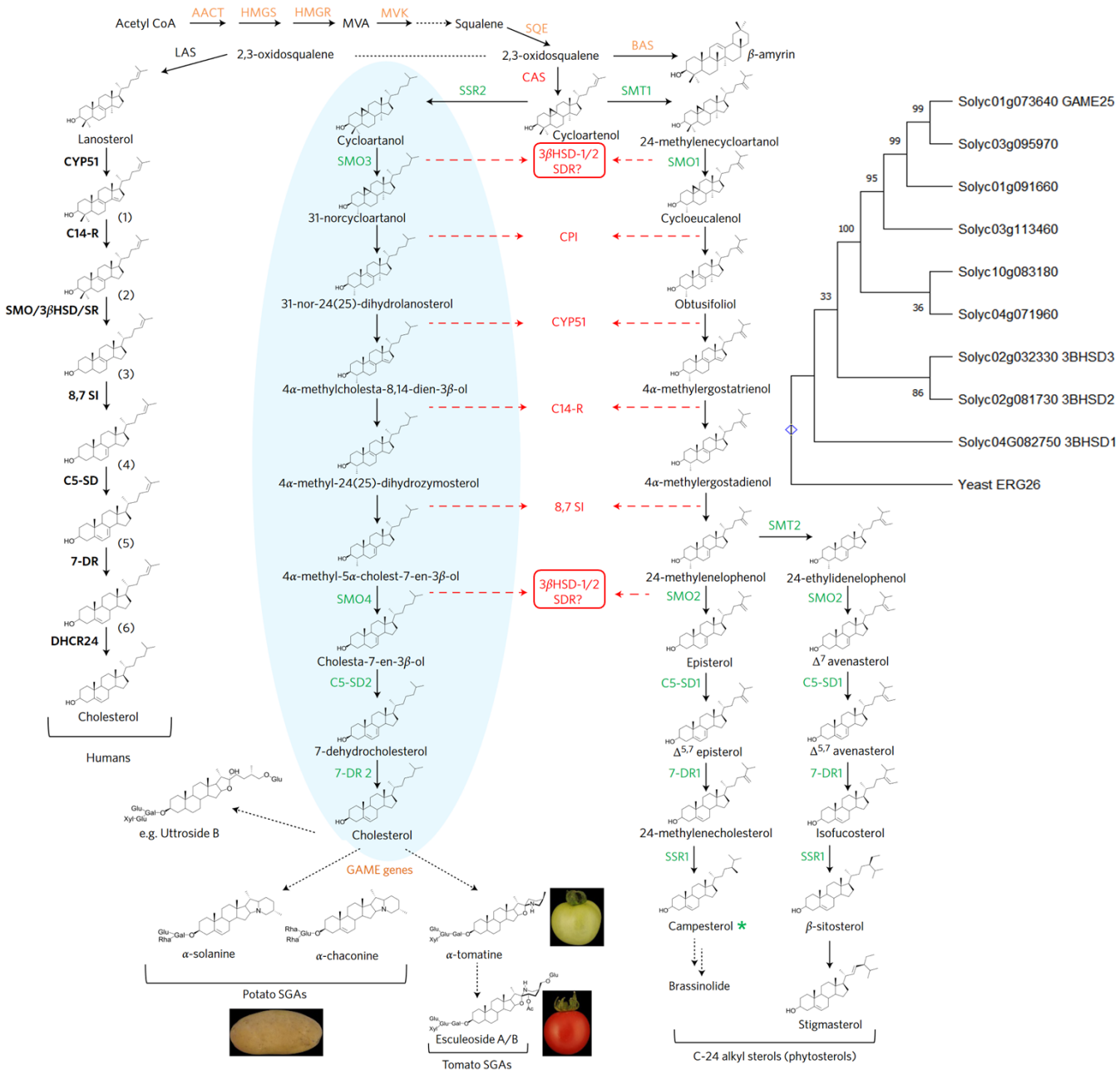

Supplemental Figure 7. The Cholesterogenesis pathway in plants and its relationship to phytosterol metabolism and cholesterogenesis in humans (via Sonawane et al., 2019) and gene tree of 3β-HSD family genes.

The plant cholesterogenesis pathway comprises ten biosynthetic steps starting from 2,3-oxidosqualene. Enzymes taking part in both the plant cholesterol andthe C-24 alkyl phytosterols biosynthetic pathways are depicted in red whereas enzymes specific for one of these pathways are marked in green; MVA, the triterpenoid precursor and other triterpenoid pathway enzymes are presented in orange. Enzymes catalysing human cholesterogenesis are shown in black and bold. Note that SMO enzymes in eukaryotes function as a complex with 3βHSD and SR. MVA, mevalonic acid; AACT, acetyl CoA acetyltransferase; HMGS, 3-hydroxy-3-methylglutaryl-CoA synthase; HMGR, 3-hydroxy-3-methylglutaryl-CoA reductase; MVK, mevalonate kinase; SQE,

squalene epoxidase; BAS, β-amyrin synthase; CAS, cycloartenol synthase; LAS, lanosterol synthase; SMT, sterol C-24 methyltransferase; SMO, C-4 sterol methyl oxidase; SDR, side chain oxidoreductase; CPI, cyclopropylsterol isomerase; CYP51, sterol C-14 demethylase; C14-R, sterol C-14 reductase; 8,7 SI, sterol 8,7 isomerase; C5-SD2, sterol C-5(6) desaturase 2; 7-DR2, 7-dehydrocholesterol reductase 2; C5-SD1, sterol C-5(6) desaturase 1 (DWARF7); 7-DR1, 7-dehydrocholesterol reductase 1 (DWARF5); SSR2, sterol side chain reductase 2; DHCR24, C24-sterol reductase. In human cholesterogenesis, the intermediates are: (1) 4,4-dimethylcholesta-8,14(15),24-trien-3β-ol; (2) 4,4-dimethylcholesta-8,24-dien-3β-ol; (3) cholesta-8,24-dien-3β-ol; (4) cholesta-7,24-dien-3β-ol, (5) 7-dehydrodesmosterol; (6) desmosterol.

Phylogenetic tree of 3β-HSD family genes in *S. lycopersicum* rooted to a homolog in *Saccharomyces cerevisiae*. Multiple alignment performed by ClutsalW using default parameters and tree generated by MegaX Maximum Likelihood algorithm with 1000 bootstrap replicates. Numbers on branches indicate bootstrap consensus percentage.

BIBIOLOGRAPHY

INTRODUCTION

Buzby, J. C., Hyman, J., Stewart, H., & Wells, H. F. (2011). The Value of Retail- and Consumer-Level Fruit and Vegetable Losses in the United States. *The Journal of Consumer Affairs*, *45*(3), 492–515.

Fich, E. A., Segerson, N. A., & Rose, J. K. C. (2016). The Plant Polyester Cutin: Biosynthesis, Structure, and Biological Roles. *Annual Review of Plant Biology*, *67*(1), 207–233. https://doi.org/10.1146/annurev-arplant-043015-111929

Martin, L. B. B., & Rose, J. K. C. (2014). There's more than one way to skin a fruit: Formation and functions of fruit cuticles. *Journal of Experimental Botany*, *65*(16), 4639–4651. https://doi.org/10.1093/jxb/eru301

Petit, J., Bres, C., Reynoud, N., Lahaye, M., Marion, D., Bakan, B., & Rothan, C. (2021). Unraveling Cuticle Formation, Structure, and Properties by Using Tomato Genetic Diversity. *Frontiers in Plant Science*, *12*, 778131. https://doi.org/10.3389/fpls.2021.778131

Philippe, G., De Bellis, D., Rose, J. K. C., & Nawrath, C. (2021). Trafficking Processes and Secretion Pathways Underlying the Formation of Plant Cuticles. *Frontiers in Plant Science*, *12*, 786874. https://doi.org/10.3389/fpls.2021.786874

Schreiber, L. (2010). Transport barriers made of cutin, suberin and associated waxes. *Trends in Plant Science*, *15*(10), 546–553. https://doi.org/10.1016/j.tplants.2010.06.004

Yeats, T. H., & Rose, J. K. C. (2013). The Formation and Function of Plant Cuticles1. *Plant Physiology*, *163*(1), 5–20. https://doi.org/10.1104/pp.113.222737

CHAPTER 1

Asami, T., Nakano, T. and Fujioka, S. (2005) Plant brassinosteroid hormones. Vitam. Horm. 72, 479-504.

Bessueille, L., Sindt, N., Guichardant, M., Djerbi, S., Teeri, T.T. and Bulone, V. (2009) Plasma membrane microdomains from hybrid aspen cells are involved in cell wall polysaccharide biosynthesis. Biochem J. 420, 93-103.

Blakeney, A.B. and Mutton, L.L. (1980) A simple colorimetric method for the determination of sugars in fruit and vegetables. J. Sci. Food Agric. 31, 889-897

Boutte, Y. and Grebe, M. (2009) Cellular processes relying on sterol function in plants. Curr. Opin. Plant Biol. 12, 705-713.

Brüeggenwirth, M., & Knoche, M. (2017). Cell wall swelling, fracture mode, and the mechanical properties of cherry fruit skins are closely related. PLANTA, 245(4), 765–777. https://doi.org/10.1007/s00425-016-2639-7

Buda, G.J., Isaacson, T., Matas, A.J., Paolillo, D.J. and Rose, J.K. (2009) Three-dimensional imaging of plant cuticle architecture using confocal scanning laser microscopy. Plant J. 60, 378-385.

Butani, A., Purohit, H., Solanki, R., Mishra, P., & Dadhaniya, D. (2019). A Chronic Problem of Fruit Cracking in Fruit Crops: A Review.

Cano-Delgado, A., Yin, Y., Yu, C., Vafeados, D., Mora-Garcia, S., Cheng, J.C., Nam, K.H., Li, J. and Chory, J. (2004) BRL1 and BRL3 are novel brassinosteroid receptors that function in vascular differentiation in Arabidopsis. Development, 131, 5341-5351.

Carland, F., Fujioka, S. and Nelson, T. (2010) The sterol methyltransferases SMT1, SMT2, and SMT3 influence Arabidopsis development through nonbrassinosteroid products. Plant Physiol. 153, 741-756.

Carland, F.M., Fujioka, S., Takatsuto, S., Yoshida, S. and Nelson, T. (2002) The identification of CVP1 reveals a role for sterols in vascular patterning. Plant Cell, 14, 2045-2058.

Carmona-Salazar, L., El Hafidi, M., Enriquez-Arredondo, C., Vazquez-Vazquez, C., Gonzalez de la Vara, L.E. and Gavilanes-Ruiz, M. (2011) Isolation of detergent-resistant membranes from plant photosynthetic and non-photosynthetic tissues. Anal. Biochem. 417, 220-227.

Chávez, A., Castillo, N., López-Tubau, J. M., Atanasov, K. E., Fernández-Crespo, E., Camañes, G., Altabella, T., & Ferrer, A. (2023). Tomato STEROL GLYCOSYLTRANSFERASE 1 silencing unveils a major role of steryl glycosides in plant and fruit development. Environmental and Experimental Botany, 206, 105181. https://doi.org/10.1016/j.envexpbot.2022.105181

Clouse, S.D. and Sasse, J.M. (1998) BRASSINOSTEROIDS: Essential regulators of plant growth and development. Annu. Rev. Plant Physiol. Plant Mol. Biol. 49, 427-451.

DeBolt, S., Scheible, W.R., Schrick, K., Auer, M., Beisson, F., Bischoff, V., Bouvier-Nave, P., Carroll, A., Hematy, K., Li, Y., Milne, J., Nair, M., Schaller, H., Zemla, M. and Somerville, C. (2009) Mutations in UDP-glucose: Sterol glucosyltransferase in Arabidopsis cause transparent testa phenotype and suberization defect in seeds. Plant Physiol. 151, 78-87.

Deng, S., Wei, T., Tan, K., Hu, M., Li, F., Zhai, Y., Ye, S., Xiao, Y., Hou, L., Pei, Y., & Luo, M. (2016). Phytosterol content and the campesterol: Sitosterol ratio influence cotton fiber development: role of phytosterols in cell elongation. Science China-Life Sciences, 59(2), 183–193. https://doi.org/10.1007/s11427-015-4992-3

Ehret, D.L. and Helmer, T. (1995) Factors contributing to cuticle cracking in greenhouse tomato fruit. HortScience, 30, 846.

Ferrer, A., Altabella, T., Arró, M., & Boronat, A. (2017). Emerging roles for conjugated sterols in plants. *Progress in Lipid Research*, *67*, 27–37. https://doi.org/10.1016/j.plipres.2017.06.002

Fich, E. A., Segerson, N. A., & Rose, J. K. C. (2016). The Plant Polyester Cutin: Biosynthesis, Structure, and Biological Roles. *Annual Review of Plant Biology*, *67*(1), 207–233. https://doi.org/10.1146/annurev-arplant-043015-111929

Foster, C.E., Martin, T.M. and Pauly, M. (2010) Comprehensive compositional analysis of plant cell walls (lignocellulosic biomass) Part II: Carbohydrates. J. Vis. Ex. 37, 1837.

Fujiwara, M., Hamada, S., Hiratsuka, M., Fukao, Y., Kawasaki, T. and Shimamoto, K. (2009) Proteome analysis of detergent-resistant membranes (DRMs) associated with OsRac1-mediated innate immunity in rice. Plant Cell Physiol. 50, 1191-1200.

Fulton, M.T., Chunwongse, J. and Tanskley, S.D. (1995) Microprep protocol for extraction of DNA from tomato and other herbaceous plants. Plant Mol. Biol. Rep. 13, 207-209.

Jackson, D.P. (1992) In-situ hybridization in plants. In Molecular Plant Pathology: A Practical Approach (Edited by Gurr, S.J., McPhereson, M. and Bowles, D.J.). Oxford: Oxford University Press, pp. 163–174.

Jang, J., Fujioka, S., Tasaka, M., Seto, H., Takatsuto, S., Ishii, A., Aida, M., Yoshida, S. and Sheen, J. (2000) A critical role of sterols in embryonic patterning and meristem programming revealed by the fackel mutants of Arabidopsis thaliana. Genes and Development, 14, 1485-1497.

Jefferson, R.A., Kavanagh, T.A. and Bevan, M.W. (1987) Gus fusions beta glucuronidase as a sensitive and versatile gene fusion marker in higher plants. EMBO (European Molecular Biology Organization) Journal, 6, 3901-3908.

Jiang, F., Lopez, A., Jeon, S., de Freitas, S. T., Yu, Q., Wu, Z., Labavitch, J. M., Tian, S., Powell, A. L. T., & Mitcham, E. (2019). Disassembly of the fruit cell wall by the ripening-associated polygalacturonase and expansin influences tomato cracking. Horticulture Research, 6, 17. https://doi.org/10.1038/s41438-018-0105-3

Jornvall, H., Persson, B., Krook, M., Atrian, S., Gonzalez-Duarte, R., Jeffery, J. and Ghosh, D. (1995) Short-chain dehydrogenases/reductases (SDR). Biochemistry, 34, 6003-6013.

Kim, B., Kim, G., Fujioka, S., Takatsuto, S., & Choe, S. (2012). Overexpression of 3β-Hydroxysteroid Dehydrogenases/C-4 Decarboxylases Causes Growth Defects Possibly Due to Abnormal Auxin Transport in Arabidopsis. Molecules and Cells, 34(1), 77–84. https://doi.org/10.1007/s10059-012-0102-6

Lee, H. J., Nakayasu, M., Akiyama, R., Kobayashi, M., Miyachi, H., Sugimoto, Y., Umemoto, N., Saito, K., Muranaka, T., & Mizutani, M. (2019). Identification of a 3 beta-Hydroxysteroid Dehydrogenase/3-Ketosteroid Reductase Involved in alpha-Tomatine Biosynthesis in Tomato. Plant and Cell Physiology, 60(6), 1304–1315. https://doi.org/10.1093/pcp/pcz049

Leide, J., Hildebrandt, U., Reussing, K., Riederer, M. and Vogg, G. (2007) The developmental pattern of tomato fruit wax accumulation and its impact on cuticular transpiration barrier properties: Effects of a deficiency in a beta-ketoacyl-coenzyme A synthase (LeCER6). Plant Physiol. 144, 1667-1679.

Leliaert, F., Verbruggen, H., & Zechman, F. W. (2011). Into the deep: New discoveries at the base of the green plant phylogeny. *BioEssays*, *33*(9), 683–692. https://doi.org/10.1002/bies.201100035

Levental, I., & Lyman, E. (2023). Regulation of membrane protein structure and function by their lipid nano-environment. Nature Reviews Molecular Cell Biology, 24(2), Article 2. https://doi.org/10.1038/s41580-022-00524-4

Li, J. (2010) Regulation of the nuclear activities of brassinosteroid signaling. Curr. Opin. Plant Biol. 13, 540-547.

Martin, L. B. B., & Rose, J. K. C. (2014). There's more than one way to skin a fruit: Formation and functions of fruit cuticles. *Journal of Experimental Botany*, *65*(16), 4639–4651. https://doi.org/10.1093/jxb/eru301

McCourt, R. M., Lewis, L. A., Strother, P. K., Delwiche, C. F., Wickett, N. J., de Vries, J., & Bowman, J. L. (2023). Green land: Multiple perspectives on green algal evolution and the earliest land plants. *American Journal of Botany*, *110*(5), e16175. https://doi.org/10.1002/ajb2.16175

Menda, N., Semel, Y., Peled, D., Eshed, Y. and Zamir, D. (2004) In silico screening of a saturated mutation library of tomato. Plant J. 38, 861-872.

Molina, I., Li-Beisson, Y., Beisson, F., Ohlrogge, J.B. and Pollard, M. (2009) Identification of an Arabidopsis feruloyl-coenzyme A transferase required for suberin synthesis. Plant Physiol. 151, 1317-1328.

Mongrand, S., Stanislas, T., Bayer, E.M., Lherminier, J. and Simon-Plas, F. (2010) Membrane rafts in plant cells. Trends Plant Sci. 15, 656-663.

Morel, J., Claverol, S., Mongrand, S., Furt, F., Fromentin, J., Bessoule, J.J., Blein, J.P. and Simon-Plas, F. (2006) Proteomics of plant detergent-resistant membranes. Mol. Cell. Proteomics, 5, 1396-1411.

Mutwil, M., Debolt, S. and Persson, S. (2008) Cellulose synthesis: A complex complex. Curr. Opin. Plant Biol. 11, 252-257.

Narita, J. O., & Gruissem, W. (1989). Tomato hydroxymethylglutaryl-CoA reductase is required early in fruit development but not during ripening. The Plant Cell, 1(2), 181–190. https://doi.org/10.1105/tpc.1.2.181

Nemhauser, J.L., Mockler, T.C. and Chory, J. (2004) Interdependency of brassinosteroid and auxin signaling in Arabidopsis. PLoS Biol. 2, 1460-1471.

Niu, Q., Tan, K., Zang, Z., Xiao, Z., Chen, K., Hu, M., & Luo, M. (2019). Modification of phytosterol composition influences cotton fiber cell elongation and secondary cell wall deposition. Bmc Plant Biology, 19, 208. https://doi.org/10.1186/s12870-019-1830-y

Ovecka, M., Berson, T., Beck, M., Derksen, J., Samaj, J., Baluska, F. and Lichtscheidl, I.K. (2010) Structural sterols are involved in both the initiation and tip growth of root hairs in Arabidopsis thaliana. Plant Cell, 22, 2999-3019.

Peet, M. M. (2009). PHYSIOLOGICAL DISORDERS IN TOMATO FRUIT DEVELOPMENT. Acta Horticulturae, 821, 151–160. https://doi.org/10.17660/ActaHortic.2009.821.16

Peng, L., Kawagoe, Y., Hogan, P., & Delmer, D. (2002). Sitosterol-β-glucoside as Primer for Cellulose Synthesis in Plants. Science, 295(5552), 147–150. https://doi.org/10.1126/science.1064281

Petit, J., Bres, C., Reynoud, N., Lahaye, M., Marion, D., Bakan, B., & Rothan, C. (2021). Unraveling Cuticle Formation, Structure, and Properties by Using Tomato Genetic Diversity. *Frontiers in Plant Science*, *12*, 778131. https://doi.org/10.3389/fpls.2021.778131

Philippe, G., De Bellis, D., Rose, J. K. C., & Nawrath, C. (2021). Trafficking Processes and Secretion Pathways Underlying the Formation of Plant Cuticles. *Frontiers in Plant Science*, *12*, 786874. https://doi.org/10.3389/fpls.2021.786874

Pose, D. and Botella, M.A. (2009) Analysis of the Arabidopsis dry2/sqe1-5 mutant suggests a role for sterols in signaling. Plant Signal Behav. 4, 873-874.

Pose, D., Castanedo, I., Borsani, O., Nieto, B., Rosado, A., Taconnat, L., Ferrer, A., Dolan, L., Valpuesta, V. and Botella, M.A. (2009) Identification of the Arabidopsis dry2/sqe1-5 mutant reveals a central role for sterols in drought tolerance and regulation of reactive oxygen species. Plant J. 59, 63-76.

Rahier, A. (2011) Dissecting the sterol C-4 demethylation process in higher plants. from structures and genes to catalytic mechanism. Steroids, 76, 340-352.

Rahier, A., Darnet, S., Bouvier, F., Camara, B., & Bard, M. (2006). Molecular and Enzymatic Characterizations of Novel Bifunctional 3β-Hydroxysteroid Dehydrogenases/C-4 Decarboxylases from Arabidopsis thaliana*. Journal of Biological Chemistry, 281(37), 27264–27277. https://doi.org/10.1074/jbc.M604431200

Rose, J.K. and Bennett, A.B. (1999) Cooperative disassembly of the cellulose-xyloglucan network of plant cell walls: Parallels between cell expansion and fruit ripening. Trends Plant Sci. 4, 176-183.

Santos, M., Egea-Cortines, M., Gonçalves, B., & Matos, M. (2023). Molecular mechanisms involved in fruit cracking: A review. Frontiers in Plant Science, 14. https://www.frontiersin.org/articles/10.3389/fpls.2023.1130857

Schaller, H. (2003) The role of sterols in plant growth and development. Prog. Lipid Res. 42, 163-175.

Schaller, H. (2004) New aspects of sterol biosynthesis in growth and development of higher plants. Plant Physiol. Biochem. 42, 465-476.

Schrick, K., Fujioka, S., Takatsuto, S., Stierhof, Y., Stransky, H., Yoshida, S. and Jurgens, G. (2004) A link between sterol biosynthesis, the cell wall, and cellulose in Arabidopsis. Plant J. 38, 227-243.

Schrick, K., Mayer, U., Horrichs, A., Kuhnt, C., Bellini, C., Dangl, J., Schmidt, J. and Jurgens, G. (2000) FACKEL is a sterol C-14 reductase required for organized cell division and expansion in Arabidopsis embryogenesis. Genes Dev. 14, 1471-1484.

Schrick, K., Mayer, U., Martin, G., Bellini, C., Kuhnt, C., Schmidt, J. and Jurgens, G. (2002) Interactions between sterol biosynthesis genes in embryonic development of Arabidopsis. Plant J. 31, 61-73.

Schrick, K., Shiva, S., Arpin, J.C., Delimont, N., Isaac, G., Tamura, P. and Welti, R. (2011) Steryl glucoside and acyl steryl glucoside analysis of Arabidopsis seeds by electrospray ionization tandem mass spectrometry. Lipids, Online First™.

Silvius, J.R. (2005) Partitioning of membrane molecules between raft and non-raft domains: Insights from model-membrane studies. Biochim. Biophys. Acta, 1746, 193-202.

Sonawane, P. D., Heinig, U., Panda, S., Gilboa, N. S., Yona, M., Kumar, S. P., Alkan, N., Unger, T., Bocobza, S., Pliner, M., Malitsky, S., Tkachev, M., Meir, S., Rogachev, I., & Aharoni, A.

(2018). Short-chain dehydrogenase/reductase governs steroidal specialized metabolites structural diversity and toxicity in the genus Solanum. Proceedings of the National Academy of Sciences of the United States of America, 115(23), E5419–E5428. https://doi.org/10.1073/pnas.1804835115

Sonawane, P. D., Pollier, J., Panda, S., Szymanski, J., Massalha, H., Yona, M., Unger, T., Malitsky, S., Arendt, P., Pauwels, L., Almekias-Siegl, E., Rogachev, I., Meir, S., Cardenas, P. D., Masri, A., Petrikov, M., Schaller, H., Schaffer, A. A., Kamble, A., … Aharoni, A. (2016). Plant cholesterol biosynthetic pathway overlaps with phytosterol metabolism. Nature Plants, 3(1), 16205. https://doi.org/10.1038/nplants.2016.205

Sørensen, I., Pettolino, F. A., Bacic, A., Ralph, J., Lu, F., O'Neill, M. A., Fei, Z., Rose, J. K. C., Domozych, D. S., & Willats, W. G. T. (2011). The charophycean green algae provide insights into the early origins of plant cell walls. *The Plant Journal: For Cell and Molecular Biology*, *68*(2), 201–211. https://doi.org/10.1111/j.1365-313X.2011.04686.x

Souter, M., Topping, J., Pullen, M., Friml, J., Palme, K., Hackett, R., Grierson, D. and Lindsey, K. (2002) Hydra mutants of Arabidopsis are defective in sterol profiles and auxin and ethylene signaling. Plant Cell, 14, 1017-1031.

Tanner, W., Malinsky, J. and Opekarova, M. (2011) In plant and animal cells, detergent-resistant membranes do not define functional membrane rafts. Plant Cell, 23, 1191-1193.

Thipyapong, P., Joel, D.M. and Steffens, J.C. (1997) Differential expression and turnover of the tomato polyphenol oxidase gene family during vegetative and reproductive development. Plant Physiol. 113, 707-718.

Thipyapong, P., Stout, M.J. and Attajarusit, J. (2007) Functional analysis of polyphenol oxidases by antisense/sense technology. Molecules, 12, 1569-1595.

Titapiwatanakun, B., Blakeslee, J.J., Bandyopadhyay, A., Yang, H., Mravec, J., Sauer, M., Cheng, Y., Adamec, J., Nagashima, A., Geisler, M., Sakai, T., Friml, J., Peer, W.A. and Murphy, A.S. (2009) ABCB19/PGP19 stabilises PIN1 in membrane microdomains in Arabidopsis. Plant J. 57, 27-44.

Valitova, J. N., Sulkarnayeva, A. G., & Minibayeva, F. V. (2016). Plant sterols: Diversity, biosynthesis, and physiological functions. Biochemistry-Moscow, 81(8), 819–834. https://doi.org/10.1134/S0006297916080046

Van Eck J., Kirk D.D. and Walmsley A.M. (2006) Tomato (lycopersicum esculentum). Methods in Molecular Biology, 343, 459-473.

Vogg, G., Fischer, S., Leide, J., Emmanuel, E., Jetter, R., Levy, A.A. and Riederer, M. (2004) Tomato fruit cuticular waxes and their effects on transpiration barrier properties: Functional characterization of a mutant deficient in a very-long-chain fatty acid beta-ketoacyl-CoA synthase. J. Exp. Bot. 55, 1401-1410.

Vrebalov, J., Pan, I.L., Arroyo, A.J., McQuinn, R., Chung, M., Poole, M., Rose, J., Seymour, G., Grandillo, S., Giovannoni, J. and Irish, V.F. (2009) Fleshy fruit expansion and ripening are regulated by the tomato SHATTERPROOF gene TAGL1. Plant Cell, 21, 3041-3062.

Wang, Y., Guo, L., Zhao, X., Zhao, Y., Hao, Z., Luo, H., & Yuan, Z. (2021). Advances in Mechanisms and Omics Pertaining to Fruit Cracking in Horticultural Plants. Agronomy, 11(6), 1045. https://doi.org/10.3390/agronomy11061045

Wang, Z.Y., Wang, Q., Chong, K., Wang, F., Wang, L., Bai, M. and Jia, C. (2006) The brassinosteroid signal transduction pathway. Cell Res. 16, 427-434.

Waters, E. R. (2003). Molecular adaptation and the origin of land plants. *Molecular Phylogenetics and Evolution*, *29*(3), 456–463. https://doi.org/10.1016/j.ympev.2003.07.018

Wewer, V., Dombrink, I., vom Dorp, K. and Dormann, P. (2011) Quantification of sterol lipids in plants by quadrupole time-of-flight mass spectrometry. J. Lipid Res. 52, 1039-1054.

Whitaker, B. D., & Gapper, N. E. (2008). Ripening-Specific Stigmasterol Increase in Tomato Fruit Is Associated with Increased Sterol C-22 Desaturase (CYP710A11) Gene Expression. Journal of Agricultural and Food Chemistry, 56(10), 3828–3835. https://doi.org/10.1021/jf7037983

Whitaker, B.D. (1991) Changes in lipids of tomato fruit stored at chilling and non-chilling temperatures. Phytochemistry (Oxford), 30, 757-762.

Whitaker, B.D. and Gapper, N.E. (2008) Ripening-specific stigmasterol increase in tomato fruit is associated with increased sterol C-22 desaturase (CYP710A11) gene expression. J. Agric. Food Chem. 56, 3828-3835.

Yeats, T. H., & Rose, J. K. C. (2013). The Formation and Function of Plant Cuticles. Plant Physiology, 163(1), 5–20. https://doi.org/10.1104/pp.113.222737

Yeats, T. H., Martin, L. B. B., Viart, H. M.-F., Isaacson, T., He, Y., Zhao, L., Matas, A. J., Buda, G. J., Domozych, D. S., Clausen, M. H., & Rose, J. K. C. (2012). The identification of cutin synthase: Formation of the plant polyester cutin. *Nature Chemical Biology*, *8*(7), 609–611. https://doi.org/10.1038/nchembio.960

Yeats, T.H., Howe, K.J., Matas, A.J., Buda, G.J., Thannhauser, T.W. and Rose, J.K.C. (2010) Mining the surface proteome of tomato (Solanum lycopersicum) fruit for proteins associated with cuticle biogenesis. J. Exp. Bot. 61, 3759-3771.

CHAPTER 2

Berhin, A., Nawrath, C., & Hachez, C. (2022). Subtle interplay between trichome development and cuticle formation in plants. *New Phytologist*, *233*(5), 2036–2046. https://doi.org/10.1111/nph.17827

Blanke, M. (1986). Comparative SEM study of stomata on developing quince, apple, grape and tomato fruit. *Angewardte Botanik*, *60*, 209–214.

Buschhaus, C., & Jetter, R. (2012). Composition and Physiological Function of the Wax Layers Coating Arabidopsis Leaves: β-Amyrin Negatively Affects the Intracuticular Water Barrier. *Plant Physiology*, *160*(2), 1120–1129. https://doi.org/10.1104/pp.112.198473

Fich, E. A., Fisher, J., Zamir, D., & Rose, J. K. C. (2020). Transpiration from Tomato Fruit Occurs Primarily via Trichome-Associated Transcuticular Polar Pores. *Plant Physiology*, *184*(4), 1840–1852. https://doi.org/10.1104/pp.20.01105

Jetter, R., & Riederer, M. (2016). Localization of the Transpiration Barrier in the Epi- and Intracuticular Waxes of Eight Plant Species: Water Transport Resistances Are Associated with Fatty Acyl Rather Than Alicyclic Components. *Plant Physiology*, *170*(2), 921–934. https://doi.org/10.1104/pp.15.01699

Jordan, W. R., Shouse, P. J., Blum, A., Miller, F. R., & Monk, R. L. (1984). Environmental Physiology of Sorghum. II. Epicuticular Wax Load and Cuticular Transpiration1. *Crop Science*, *24*(6), cropsci1984.0011183X002400060038x. https://doi.org/10.2135/cropsci1984.0011183X002400060038x

Leide, J., Hildebrandt, U., Vogg, G., & Riederer, M. (2011). The positional sterile (ps) mutation affects cuticular transpiration and wax biosynthesis of tomato fruits. *Journal of Plant Physiology*, *168*(9), 871–877. https://doi.org/10.1016/j.jplph.2010.11.014

Luckwill, L. C. (Ed.). (n.d.). *The genus Lycopersicon: An historical, biological, and taxonomic survery of the wild and cultivated tomatoes*. Aberdeen University Press.

Martin, L. B. B., & Rose, J. K. C. (2014). There's more than one way to skin a fruit: Formation and functions of fruit cuticles. *Journal of Experimental Botany*, *65*(16), 4639–4651. https://doi.org/10.1093/jxb/eru301

Parsons, E. P., Popopvsky, S., Lohrey, G. T., Alkalai-Tuvia, S., Perzelan, Y., Bosland, P., Bebeli, P. J., Paran, I., Fallik, E., & Jenks, M. A. (2013). Fruit cuticle lipid composition and water loss in a diverse collection of pepper (Capsicum). *Physiologia Plantarum*, *149*(2), 160–174. https://doi.org/10.1111/ppl.12035

Paul, V., & Srivastava, G. (2006). Role of surface morphology in determining the ripening behaviour of tomato (Lycopersicon esculentum Mill.) fruits. *Scientia Horticulturae*, *110*, 84–92. https://doi.org/10.1016/j.scienta.2006.06.023

Philippe, G., Sørensen, I., Jiao, C., Sun, X., Fei, Z., Domozych, D. S., & Rose, J. K. (2020). Cutin and suberin: Assembly and origins of specialized lipidic cell wall scaffolds. *Current Opinion in Plant Biology*, *55*, 11–20. https://doi.org/10.1016/j.pbi.2020.01.008

Ramírez, F., & Davenport, T. L. (2020). The Development of Lulo Plants (*Solanum quitoense* Lam. Var. *Septentrionale*) Characterized by BBCH and Landmark Phenological Scales. *International Journal of Fruit Science*, *20*(3), 562–585. https://doi.org/10.1080/15538362.2019.1613470

Riederer, M., & Schreiber, L. (2001). Protecting against water loss: Analysis of the barrier properties of plant cuticles. *Journal of Experimental Botany*, *52*(363), 2023–2032. https://doi.org/10.1093/jexbot/52.363.2023

Šantrůček, J., Šimáňová, E., Karbulková, J., Šimková, M., & Schreiber, L. (2004). A new technique for measurement of water permeability of stomatous cuticular membranes isolated from Hedera helix leaves. *Journal of Experimental Botany*, *55*(401), 1411–1422. https://doi.org/10.1093/jxb/erh150

Schreiber, L. (2010). Transport barriers made of cutin, suberin and associated waxes. *Trends in Plant Science*, *15*(10), 546–553. https://doi.org/10.1016/j.tplants.2010.06.004

Schreiber, L., & Riederer, M. (1996). Ecophysiology of cuticular transpiration: Comparative investigation of cuticular water permeability of plant species from different habitats. *Oecologia*, *107*(4), 426–432. https://doi.org/10.1007/BF00333931

Shen, Y., Li, X., Xiong, R., Ni, Y., Tian, S., & Li, B. (2023). Effect of peach trichome removal on post-harvest brown rot and on the fruit surface microbiome. *International Journal of Food Microbiology*, *402*, 110299. https://doi.org/10.1016/j.ijfoodmicro.2023.110299

Simmons, A. T., & Gurr, G. M. (2005). Trichomes of Lycopersicon species and their hybrids: Effects on pests and natural enemies. *Agricultural and Forest Entomology*, *7*(4), 265–276. https://doi.org/10.1111/j.1461-9555.2005.00271.x

Ursache, R., Andersen, T. G., Marhavý, P., & Geldner, N. (2018). A protocol for combining fluorescent proteins with histological stains for diverse cell wall components. *The Plant Journal*, *93*(2), 399–412. https://doi.org/10.1111/tpj.13784

Vogg, G., Fischer, S., Leide, J., Emmanuel, E., Jetter, R., Levy, A. A., & Riederer, M. (2004). Tomato fruit cuticular waxes and their effects on transpiration barrier properties: Functional characterization of a mutant deficient in a very-long-chain fatty acid -ketoacyl-CoA synthase. *Journal of Experimental Botany*, *55*(401), 1401–1410. https://doi.org/10.1093/jxb/erh149

Wang, D.-J., Zeng, J.-W., Ma, W.-T., Lu, M., & An, H.-M. (2019). Morphological and Structural Characters of Trichomes on Various Organs of Rosa roxburghii. *HortScience*, *54*(1), 45–51. https://doi.org/10.21273/HORTSCI13485-18

Wang, X., Shen, C., Meng, P., Tan, G., & Lv, L. (2021). Analysis and review of trichomes in plants. *BMC Plant Biology*, *21*(1), 70. https://doi.org/10.1186/s12870-021-02840-x

Watts, S., & Kariyat, R. (2021). Morphological characterization of trichomes shows enormous variation in shape, density and dimensions across the leaves of 14 Solanum species. *AoB Plants*, *13*(6), plab071. https://doi.org/10.1093/aobpla/plab071

Xue, S., Dong, M., Liu, X., Xu, S., Pang, J., Zhang, W., Weng, Y., & Ren, H. (2019). Classification of fruit trichomes in cucumber and effects of plant hormones on type II fruit trichome development. *Planta*, *249*(2), 407–416. https://doi.org/10.1007/s00425-018-3004-9

Yan, R., Gurtler, J. B., Mattheis, J. P., & Fan, X. (2020). Effect of Trichome Removal and UV-C on Populations of E. coli 0157:H7 and Quality of Peach Fruit. *Hortscience*, *55*(10), 1626–1631. https://doi.org/10.21273/HORTSCI15231-20

Yeats, T. H., & Rose, J. K. C. (2013). The formation and function of plant cuticles. *Plant Physiology*, *163*(1), 5–20. https://doi.org/10.1104/pp.113.222737